

Article

Study on the Removal Characteristics of IBP and DCF in Wastewater by CW-MFC with Different Co-Substrates

Ge Qin ^{1,2,†}, Hongyu Feng ^{1,3,†} , Rendong Yu ¹, Fuchao Zheng ^{1,4}, Xufei Jiang ¹, Lu Xia ^{1,3,*} and Shuqing An ^{1,3,*}¹ School of Life Science and Institute of Wetland Ecology, Nanjing University, Nanjing 210023, China² School of Life Science and Basic Medicine, Xinxiang University, Xinxiang 453003, China³ Nanjing University Ecology Research Institute of Changshu, Changshu 210051, China⁴ Ministry of Education's Key Laboratory of Poyang Lake Wetland and Watershed Research,

School of Geography and Environment, Jiangxi Normal University, Ziyang Road 99, Nanchang 330022, China

* Correspondence: lulu8668@yeah.net (L.X.); anshq@nju.edu.cn (S.A.)

† These authors contributed equally to this work.

Abstract: Pharmaceuticals and Personal Care Products (PPCPs) constitute a group of compounds that are challenging to break down and potentially pose risks to both ecosystems and human health when they accumulate in water bodies. This study established and operated small-scale constructed wetland–microbial fuel cells (CW-MFCs) continuously for 60 days, maintaining a hydraulic retention time (HRT) of 3 days. The research aimed to assess the treatment efficiency of wastewater containing Ibuprofen (IBP) and Diclofenac (DCF) using different co-substrates (glucose, sucrose, and sodium acetate) and to analyze the impact of these co-substrates on the composition of bacterial communities within the CW-MFC. After 60 days of operation, CW-MFC achieved removal rates of 89.29% for IBP and 84.10% for DCF. The elimination of IBP was primarily dependent on co-metabolic degradation processes occurring in both the anode and cathode, while DCF removal relied on anodic co-metabolism. Additionally, various co-substrates have an influence on the bacterial community diversity of the anode and cathodes. The possible bacterial groups involved in PPCP degradation were identified. In summary, Glu was identified as a more suitable co-substrate for CW-MFC in the removal of IBP and DCF, while SA as a co-substrate favored the induction and enrichment of EAB in the anodes. These findings offer valuable insights into the potential of CW-MFC for mitigating emerging contaminants.

Keywords: constructed wetlands; constructed wetland–microbial fuel cells; PPCPs; co-metabolic; Ibuprofen; diclofenac



Citation: Qin, G.; Feng, H.; Yu, R.; Zheng, F.; Jiang, X.; Xia, L.; An, S. Study on the Removal Characteristics of IBP and DCF in Wastewater by CW-MFC with Different Co-Substrates. *Water* **2023**, *15*, 3862. <https://doi.org/10.3390/w15213862>

Academic Editor: Antonio Panico

Received: 13 October 2023

Revised: 25 October 2023

Accepted: 29 October 2023

Published: 6 November 2023



Copyright: © 2023 by the authors. Licensee MDPI, Basel, Switzerland. This article is an open access article distributed under the terms and conditions of the Creative Commons Attribution (CC BY) license (<https://creativecommons.org/licenses/by/4.0/>).

1. Introduction

Pharmaceutical and personal care products (PPCPs) comprise chemical compounds used for maintaining human health and hygiene, as well as promoting livestock health and growth. PPCPs are extensively utilized in medical, industrial, animal husbandry, aquaculture, and various other domains, intricately interwoven with everyday human life [1,2]. Most pharmaceuticals are not fully metabolized in humans or animals; their metabolites and parent compounds are excreted and enter the sewage system [3,4]. Moreover, inadequately treated medical wastewater can result in the accumulation of PPCPs in natural water bodies [5]. While environmental concentrations of these components typically fall within a low range (a few nanograms to a few micrograms per liter), their toxicity and persistence result in bioconcentration in aquatic organisms, leading to mutagenic, reproductive, genotoxic, and carcinogenic effects, thus posing a potential risk to human health [6,7]. In recent years, propelled by rapid economic growth, the PPCP production and consumption of China have assumed a leading global position [8]. The main source of PPCP infusion into the environment is through wastewater treatment plants (WWTPs), due

to the lack of necessary treatments [9,10]. PPCPs and their metabolites have been detected in numerous aqueous environments, including the presence of IBP and DCF [5,8,11].

IBP is a commonly utilized non-steroidal anti-inflammatory drug (NSAID) known for its antipyretic and analgesic properties, with an annual production of 15,000 metric tons [12]. DCF is another non-steroidal drug used to treat conditions such as pain, dysmenorrhea, ocular inflammation, osteoarthritis, rheumatoid arthritis, ankylosing spondylitis, and actinic keratosis [13]. DCF is administered orally at a daily dosage of 75–150 mg, of which around 15% is excreted unchanged into wastewater treatment systems [14,15], making it a primary source of DCF residues in urban sewage [16]. Owing to the extensive use and continuous release of IBP and DCF, substantial residue levels are often identified in raw wastewater, groundwater, surface water, and treated effluent [17], leading to adverse ecological effects. For example, the previous study found that human ovarian explants exposure to 10–100 $\mu\text{mol L}^{-1}$ IBP triggered apoptosis and reduced proliferating cells [18]. The environmental presence of DCF is a significant factor contributing to the rapid decline in the population of vultures in Pakistan [19]. Furthermore, instances of adverse human health effects resulting from fish consumption have been reported in Finland, primarily due to the presence of DCF and IBP in bile at concentrations ranging from 29 to 194 $\mu\text{g L}^{-1}$ [20]. Hence, it is imperative to effectively degrade IBP and DCF residues in the aquatic environment to ensure water safety.

Various technologies have been adopted to remove pollutants from water, such as advanced oxidation, late biological treatment, membrane separation, precipitation, and adsorption [21]. Constructed wetlands (CWs), being a relatively mature wastewater treatment technology, employ a range of physical, chemical, and biological processes to handle various types of wastewater [22,23]. In recent decades, CWs have gained increasing attention due to their ease of design and construction as well as their low operating and maintenance costs [24]. CWs have found widespread application in treating industrial wastewater, municipal domestic wastewater, dairy effluents, and textile dye wastewater [25–28]. Nevertheless, prolonged operation of CWs can lead to a decline in sewage treatment performance due to internal blockages [29]. Recently, the integration or combination of CWs with other treatment methods has been used to address these limitations, thereby improving the removal efficiency of PPCPs and mitigating environmental risks. CW-MFC, a novel integrated application, combines CWs with Microbial Fuel Cells (MFCs), allowing for concurrent wastewater treatment and energy generation [30,31]. CW-MFC combines the three PPCPS removal methods of traditional physics, chemistry, and biology [32], and also has advantages in reducing adsorption material costs and land use [33]. The introduction of MFC strengthens the performance of the anaerobic zone within the CWs [34], which is beneficial to wastewater treatment and adaptation to low temperature conditions [35]. This technology has been applied to treat wastewater containing PPCPs [36,37].

Microorganisms within CW-MFCs exert a dual influence, contributing not only to the generation of electrical energy but also serving a critical role in the removal of pollutants from wastewater [38]. Generally, microorganisms tend to aggregate in both the anode and cathode regions of the CW-MFC. Electrochemically active bacteria (EAB), capable of electricity generation, are typically more abundant in the anaerobic anode region [32]. EAB can directly metabolize simple organic compounds in wastewater to achieve pollutant removal. Nevertheless, in the case of complexly structured pollutants, they collaborate with non-EAB microorganisms to hydrolyze or ferment these compounds into simpler structures. Microorganisms fulfill an indispensable and pivotal role in the pollutant degradation processes in both CW and CW-MFC systems [39]. Nevertheless, the degradation efficiency of microorganisms towards pollutants is influenced by the operational mode and structure of the CW-MFC. Fluctuations in pollutant concentrations can also lead to different microbial degradation patterns [40,41]. Furthermore, as pollutants accumulate within the CW-MFC, the microbial community undergoes a gradual transition toward a composition better suited for pollutant degradation [42]. However, it remains unclear how IBP and DCF impact the microbial community structure within the CW-MFC.

The concentrations of detected PPCPs in natural aquatic environments are relatively low. Despite the variety of PPCP types identified, they are still insufficient to support the growth and metabolic needs of microorganisms [43]. PPCPs need to form synergistic metabolic pathways with other pollutants [44]. Meanwhile, numerous easily degradable small organic compounds can serve as co-substrates for microbial utilization in the removal of PPCPs [45–47]. In a study investigating the co-metabolic degradation of the organophosphorus pesticide malathion by *Pseudomonas*, it was observed that sodium succinate and sodium acetate facilitated both malathion biodegradation and bacterial growth, resulting in an almost complete malathion degradation rate of nearly 100%. In contrast, glucose and fructose exhibited a weak co-metabolism effect, with a malathion degradation rate of less than 30% [48]. In MFC systems, the selection of co-substrate has an influence on both pollutant removal efficiency and power generation performance [49–51]. Furthermore, diverse co-substrates can result in varying electron acceptors in CW-MFC systems. For instance, when there are high concentrations of nitrite, nitrate, and oxygen present in the system, the electrons generated by the electricity-producing bacteria may be substantially depleted, leading to a decrease in the electricity generation performance of the CW-MFC [52,53]. Therefore, bench-scale CW-MFCs were employed in this study to investigate the removal characteristics of PPCPs, specifically IBP and DCF, from simulated domestic sewage. We aimed to assess (1) the removal efficiency of IBP and DCF by CW-MFC when utilizing three distinct carbon sources (namely, glucose, succinic acid, and sucrose) as co-substrates; (2) the composition of bacterial communities in the anode and cathode.

2. Methods

2.1. Establishment and Operation of the CW-MFC

Three small-scale CW-MFC devices were built within cylindrical PVC barrels, each with a bottom diameter of 20 cm and a height of 45 cm. Gravel with a diameter of 4–6 mm is used as the bottom layer, and the thickness is 15 cm [54]. On top of this layer, a 5 cm layer of activated carbon particles (with a particle diameter of 2–3 mm) was placed to serve as the anode. A stainless steel mesh was incorporated within the activated carbon to form a stainless steel-activated carbon anode [53]. Above the anode, gravel with a thickness of 20 cm acts as the middle layer. Above the middle layer is the cathode with the same structure as the anode, and the surface of the cathode is exposed to the air. *Iris pseudacorus* was planted in the cathode area, with three plants in each reactor. Sampling ports were installed at 5 cm intervals along the side of the device, resulting in an effective volume of 3.56 L. The anode and cathode areas were connected via copper wires and connected in series with an external electrical resistor (1000 Ω) (Figure 1). A data acquisition module (DAM-3057, Art Technology Co. Ltd., Beijing, China) was employed for continuous voltage monitoring, with data acquisition occurring at 10-s intervals [55].

The CW-MFC devices were named CM-A, CM-B, and CM-C, employing glucose (Glu), sucrose (Suc), and sodium acetate (SA) as carbon sources, respectively. The carbon source was introduced into the simulated wastewater at a concentration of 300 mg·L⁻¹ (comprising Glu 282.00 mg·L⁻¹, Suc 267.30 mg·L⁻¹, SA 384.00 mg·L⁻¹). For the anode biofilm in this study, activated sludge (MLSS = 17 g·L⁻¹) was collected from the secondary sedimentation tank of the Tangshan WWTP in Nanjing. The composition of other components was as follows: NH₄Cl 133.7 mg·L⁻¹, NaH₂PO₄·2H₂O 497 mg·L⁻¹, Na₂HPO₄·12H₂O 75 mg·L⁻¹, KCl 130 mg·L⁻¹, NaHCO₃ 313 mg·L⁻¹, and MgSO₄·7H₂O 25 mg·L⁻¹. The devices were covered with tin foil to prevent the formation of microalgae, and all devices and water tanks were kept indoors at a constant room temperature of 25 °C.

During the operation of the system, a hydraulic retention time (HRT) of 3 days was established. The output voltage of the CW-MFC devices was continuously monitored through a data acquisition module. In this study, the electricity generation was stable after 30 days, with the output voltage of the CW-MFC remaining at 480 ± 5 mV. At this point, the target PPCPs, IBP, and DCF were introduced into the simulated wastewater for subsequent experiments.

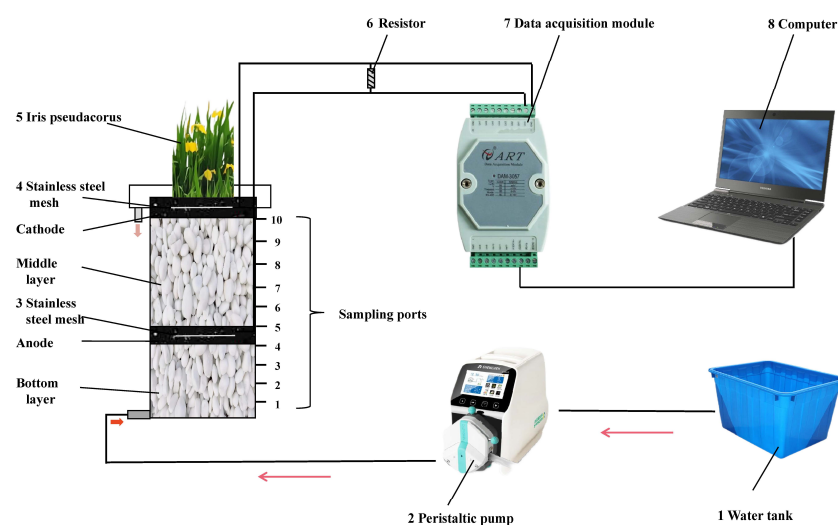


Figure 1. The schematic diagram of CW-MFC (1 water tank; 2 peristaltic pump; 3&4 stainless steel mesh; 5 *Iris pseudacorus*; 6 resistor; 7 data acquisition module; 8 computer).

IBP and DCF (Figure 2), each at a concentration of $10 \text{ mg}\cdot\text{L}^{-1}$, were introduced into the simulated wastewater, and the HRT was set at 3 days. The systems operated continuously for 60 days. The target PPCPs, IBP, and DCF (all > 98% purity) used in this study were sourced from Aladdin (Shanghai, China). Properties of the target PPCPs can be found in Table S1.

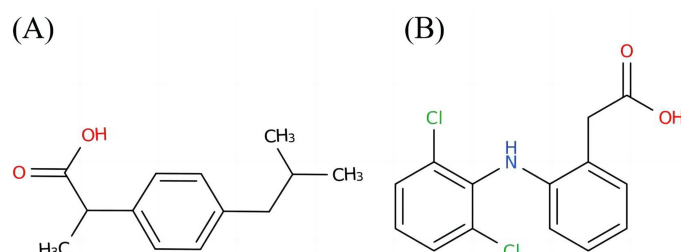


Figure 2. The chemical structures of IBP (A) and DCF (B).

2.2. Water Sampling and Analysis

Triplicate samples were collected from the sampling points 1, 4, 5, and the effluent, as depicted in Figure 1, every 10 days. The concentrations of COD, total nitrogen (TN), ammonium ($\text{NH}_4^+\text{-N}$), and total phosphorus (TP) in the collected samples were analyzed by the methodology reported by [56]. Furthermore, the concentrations of PPCPs were measured using high-performance liquid chromatography (HPLC) (waters 2695, USA) with a C18 reversed-phase column Diamonsil C18(2) ($250 \times 4.6 \text{ mm}$, $5 \mu\text{m}$). For IBP, the mobile phase consisted of acetonitrile and a $0.1 \text{ mol}\cdot\text{L}^{-1}$ potassium dihydrogen phosphate aqueous solution (pH 4.0) with an isocratic elution ratio of acetonitrile to the aqueous solution of 63:37, and the detection wavelength was 263 nm, the flow rate was maintained at $1.0 \text{ mL}\cdot\text{min}^{-1}$, and the column temperature was $30 \text{ }^\circ\text{C}$. Each sample injection volume was $10 \mu\text{L}$. For DCF, a mobile phase of 4% glacial acetic acid and methanol was used with an isocratic elution ratio of 4% glacial acetic acid to methanol at 30:70, and the detection wavelength was 276 nm, the flow rate was $1.0 \text{ mL}\cdot\text{min}^{-1}$, the column temperature was $30 \text{ }^\circ\text{C}$, and the sample volume was $20 \mu\text{L}$. The standard curves for IBP and DCF are shown in Figure S1.

The power density curve and the polarization curve were employed to assess the electrical characteristics of CW-MFCs. The anode coulombic efficiency (CE) was calculated as follows [57]:

$$\text{CE} = \frac{I}{F \times q \times n \times \Delta\text{COD}}$$

I is the current (A), F is the Faraday constant (96485 C/mol e⁻), 32 is the molar mass of O₂, 4 is the electron number gained by the reduction reaction of 1 molar O₂, q is volumetric influent flow rate of CW-MFCs (L/s), and ΔCOD is the difference of COD between the influent and the effluent of the anode.

2.3. Substrate Sampling and Bacterial Community Analysis

The activated carbon from the anode and cathode of the CW-MFC devices were sampled at the conclusion of the experiment. The E.Z.N.A.[®] soil DNA kit (Omega Bio-tek, Norcross, GA, USA) was used to extract the total DNA. The forward primer (5'-GTGCCAGCMGCCGCGG-3') and reverse primer (5'-CCGTCAATTCMTTTRAGTTT-3') were used to amplify the V4 and V5 regions of the bacterial 16S rRNA gene. The PCR protocol followed the method reported by [58]. After the amplicons were purified and quantified, high-throughput sequencing was conducted via the Illumina Miseq PE300 platform (Majorbio Bio-pharm Technology Co., Ltd., Shanghai, China). A representative sequence from each operational taxonomic unit (OTU) (sequence similarity was over 97%) was classified and assigned to a phylum, class, and genus level. Subsequently, alpha diversity indices, such as Shannon, Simpson, Ace, and Coverage, were calculated to assess the variations in the diversity and richness of bacterial communities within the devices.

2.4. Statistical Analysis

SPSS 24.0 (IBM SPSS Inc., Chicago, IL, USA) was used for statistical data analysis, and one-way analysis of variance (ANOVA) was used to analyze the differences in bacterial diversities. The IBP and DCF removal amounts between groups were compared using one-way ANOVA ($p < 0.05$) followed by Duncan's multiple range tests.

3. Results

3.1. PPCP Removal with Different Co-Substrates

The average IBP concentrations at sampling port 4 were 8.10 ± 0.04 mg L⁻¹ in devices of CM-A, 7.93 ± 0.07 mg L⁻¹ in devices of CM-C, and 8.36 ± 0.03 mg L⁻¹ in devices of CM-B (Table 1). Meanwhile, the mean values of the IBP concentrations at sampling port 5 were 2.96 ± 0.03 mg L⁻¹ in devices of CM-A, 2.21 ± 0.05 mg L⁻¹ in devices of CM-C, and 2.71 ± 0.02 mg L⁻¹ in devices of CM-B (Table 1). The IBP concentrations at sampling ports 4 and 5 in devices of various carbon sources were observably different ($p < 0.05$; Table 1). Additionally, 2.68 ± 0.04 mg L⁻¹, 2.13 ± 0.08 mg L⁻¹, and 2.63 ± 0.02 mg L⁻¹ were observed at sampling port 10 in devices of CM-A, CM-C, and CM-B, respectively (Table 1). The IBP concentrations at sampling port 10 in devices of CM-C were significantly lower than those in devices of CM-A and CM-B ($p < 0.05$; Table 1).

Table 1. IBP concentration of sampling ports and effluent using different carbon sources (mean \pm SD, $n = 3$, the initial concentration of IBP is 10 mg·L⁻¹. Uppercase and lowercase letters represent intra-group and inter-group differences, respectively. Different letters indicate significant differences, with $p < 0.05$).

Sample	IBP Concentration (mg·L ⁻¹)				
	Sampling Port 4	Sampling Port 5	Sampling Port 10	Effluent	Total Removal
CM-A (IBP-Glu)	8.10 ± 0.04 ^{Ab}	2.96 ± 0.03 ^{Ba}	2.68 ± 0.04 ^{Ca}	0.86 ± 0.04 ^{Dc}	9.14 ± 0.04 ^a
CM-C (IBP-SA)	7.93 ± 0.07 ^{Ac}	2.21 ± 0.05 ^{Bc}	2.13 ± 0.08 ^{Bb}	1.28 ± 0.05 ^{Ca}	8.72 ± 0.05 ^c
CM-B (IBP-Suc)	8.36 ± 0.03 ^{Aa}	2.71 ± 0.02 ^{Bb}	2.63 ± 0.02 ^{Ca}	1.08 ± 0.05 ^{Db}	8.92 ± 0.05 ^b

Additionally, the IBP concentrations in the final effluent liquid were 1.56 ± 0.03 mg L⁻¹, 1.64 ± 0.03 mg L⁻¹, and 1.57 ± 0.03 mg L⁻¹ in devices of CM-A, CM-C, and CM-B, respectively (Table 1). The IBP concentrations of the final effluent liquid in devices of

various carbon sources were markedly different ($p < 0.05$), indicating that the total IBP removal was highest in devices of CM-A and lowest in devices of CM-C (Table 1).

The average DCF concentrations at sampling port 4 were $6.53 \pm 0.13 \text{ mg L}^{-1}$ in devices of CM-A, $5.85 \pm 0.09 \text{ mg L}^{-1}$ in devices of CM-C, and $6.19 \pm 0.01 \text{ mg L}^{-1}$ in devices of CM-B (Table 2). Notably, there were significant differences in DCF concentrations at sampling port 4 among devices with varying carbon sources ($p < 0.05$; Table 2). At sampling port 5, the DCF concentrations were $2.67 \pm 0.18 \text{ mg L}^{-1}$ in devices of CM-A, $2.47 \pm 0.09 \text{ mg L}^{-1}$ in devices of CM-C, and $2.35 \pm 0.06 \text{ mg L}^{-1}$ in devices of CM-B, while at sampling port 10, they were $1.82 \pm 0.03 \text{ mg L}^{-1}$ in devices of CM-A, $1.71 \pm 0.02 \text{ mg L}^{-1}$ in devices of CM-C, and $1.69 \pm 0.03 \text{ mg L}^{-1}$ in devices of CM-B (Table 2). In both sampling ports 5 and 10, DCF concentrations in devices of CM-A were significantly higher compared to those in devices of CM-C and CM-B ($p < 0.05$; Table 2).

Table 2. DCF concentration of removal of sampling ports and effluent using different carbon sources (mean \pm SD, $n = 3$, the initial concentration of DCF is $10 \text{ mg} \cdot \text{L}^{-1}$. Uppercase and lowercase letters represent intra-group and inter-group differences, respectively. Different letters indicate significant differences, with $p < 0.05$).

Sample	DCF Concentration ($\text{mg} \cdot \text{L}^{-1}$)				
	Sampling Port 4	Sampling Port 5	Sampling Port 10	Effluent	Total Removal
CM-A (DCF-Glu)	$6.53 \pm 0.13^{\text{Aa}}$	$2.67 \pm 0.18^{\text{Ba}}$	$1.82 \pm 0.03^{\text{Ca}}$	$1.56 \pm 0.03^{\text{Db}}$	$8.44 \pm 0.03^{\text{a}}$
CM-C (DCF-SA)	$5.85 \pm 0.09^{\text{Ac}}$	$2.47 \pm 0.09^{\text{Bb}}$	$1.71 \pm 0.02^{\text{Cb}}$	$1.64 \pm 0.03^{\text{Ca}}$	$8.36 \pm 0.03^{\text{b}}$
CM-B (DCF-Suc)	$6.19 \pm 0.01^{\text{Ab}}$	$2.35 \pm 0.06^{\text{Bb}}$	$1.69 \pm 0.03^{\text{Cb}}$	$1.57 \pm 0.03^{\text{Db}}$	$8.43 \pm 0.03^{\text{a}}$

3.2. Bacterial Community Analysis

Bacterial community relative abundances and diversity index values were compared for various co-substrate combinations (Table 3). The coverage value of each sample exceeded 0.98. However, when SA was used as a co-substrate, the OTU numbers, alpha diversity, and uniformity were found to be significantly lower ($p < 0.05$, Table 3).

Table 3. Microbial diversity indices of samples in CW-MFC systems. Note: Observed bacterial community richness is based on the OTUs in each sample (Mean \pm SD, $n = 3$); values with superscript letters a, b, and c are significantly different between groups ($p < 0.05$).

PPCPs	Electrodes	Co-Substrates	Sobs	Shannon	Simpson	Ace	Chao	Coverage
IBP	Anode	Glu	$2881.33 \pm 49.01^{\text{a}}$	$5.87 \pm 0.24^{\text{a}}$	$0.03 \pm 0.01^{\text{a}}$	$3892.87 \pm 105.76^{\text{a}}$	$3825.06 \pm 56.04^{\text{a}}$	$0.98 \pm 0.00^{\text{a}}$
		Suc	$2757.00 \pm 52.72^{\text{a}}$	$6.23 \pm 0.03^{\text{a}}$	$0.01 \pm 0.00^{\text{a}}$	$3794.56 \pm 142.26^{\text{a}}$	$3796.97 \pm 141.16^{\text{a}}$	$0.98 \pm 0.00^{\text{a}}$
		SA	$2762.00 \pm 254.21^{\text{a}}$	$5.93 \pm 0.36^{\text{a}}$	$0.03 \pm 0.02^{\text{a}}$	$3831.85 \pm 275.12^{\text{a}}$	$3799.76 \pm 274.84^{\text{a}}$	$0.97 \pm 0.00^{\text{a}}$
	Cathode	Glu	$1749.33 \pm 1029.82^{\text{a}}$	$4.81 \pm 0.51^{\text{a}}$	$0.09 \pm 0.11^{\text{a}}$	$2184.98 \pm 1455.08^{\text{a}}$	$2189.47 \pm 1424.96^{\text{a}}$	$0.99 \pm 0.01^{\text{a}}$
		Suc	$1203.33 \pm 238.83^{\text{a}}$	$4.78 \pm 0.52^{\text{a}}$	$0.04 \pm 0.02^{\text{a}}$	$1537.54 \pm 391.85^{\text{a}}$	$1539.05 \pm 390.24^{\text{a}}$	$0.99 \pm 0.00^{\text{a}}$
		SA	$1283.67 \pm 136.45^{\text{a}}$	$4.74 \pm 0.20^{\text{a}}$	$0.04 \pm 0.01^{\text{a}}$	$1695.22 \pm 231.98^{\text{a}}$	$1704.14 \pm 243.42^{\text{a}}$	$0.99 \pm 0.00^{\text{a}}$
DCF	Anode	Glu	$2756.00 \pm 352.74^{\text{a}}$	$6.17 \pm 0.25^{\text{a}}$	$0.01 \pm 0.01^{\text{b}}$	$3698.78 \pm 357.71^{\text{ab}}$	$3701.06 \pm 349.67^{\text{b}}$	$0.98 \pm 0.00^{\text{a}}$
		Suc	$3063.67 \pm 101.66^{\text{a}}$	$6.39 \pm 0.20^{\text{a}}$	$0.01 \pm 0.00^{\text{b}}$	$4198.98 \pm 55.07^{\text{a}}$	$4204.49 \pm 91.35^{\text{a}}$	$0.97 \pm 0.00^{\text{a}}$
		SA	$2076.00 \pm 107.14^{\text{b}}$	$4.35 \pm 0.51^{\text{b}}$	$0.17 \pm 0.07^{\text{a}}$	$3486.38 \pm 310.01^{\text{b}}$	$3035.99 \pm 55.31^{\text{c}}$	$0.97 \pm 0.00^{\text{a}}$
	Cathode	Glu	$1524.33 \pm 64.84^{\text{a}}$	$5.18 \pm 0.11^{\text{a}}$	$0.02 \pm 0.00^{\text{b}}$	$1958.90 \pm 14.05^{\text{a}}$	$1921.94 \pm 7.78^{\text{a}}$	$0.99 \pm 0.00^{\text{a}}$
		Suc	$1616.67 \pm 214.28^{\text{a}}$	$5.42 \pm 0.17^{\text{a}}$	$0.02 \pm 0.00^{\text{b}}$	$2228.25 \pm 285.18^{\text{a}}$	$2218.17 \pm 307.39^{\text{b}}$	$0.98 \pm 0.00^{\text{b}}$
		SA	$1124.00 \pm 226.10^{\text{b}}$	$4.26 \pm 0.50^{\text{b}}$	$0.05 \pm 0.02^{\text{a}}$	$1642.83 \pm 429.71^{\text{a}}$	$1569.71 \pm 239.39^{\text{a}}$	$0.99 \pm 0.00^{\text{a}}$

In IBP-Glu (Figure 3A), the anode exhibits an enrichment of bacteria from four major groups, namely *Chloroflexi* (the class of *Anaerolineae*), *Verrucomicrobiota* (including the classes *Lentisphaeria* and *Omnitrophia*), *Bacteroidota* (from phylum to class), and unclassified phyla (from phylum to class). In contrast, the cathode is enriched with bacteria from the *Proteobacteria* (including the classes *Alphaproteobacteria* and *Gammaproteobacteria*), FW113 (from phylum to class), and the class *Actinobacteria*. In IBP-Suc (Figure 3B), the anode is predominantly enriched with *Chloroflexi* (from phylum to class), specifically the class

Anaerolineae (within the phylum *Chloroflexi*), *Bacteroidota* (from phylum to class), *Desulfobacterota*, *Actinobacteriota*, *Verrucomicrobiota*, and *Firmicutes*. Interestingly, the IBP-Suc cathode does not exhibit enrichment of FW113, and its community composition mirrors that of IBP-Glu (Figure 3A). In IBP-SA (Figure 3C), the anode is still dominantly occupied by *Chloroflexi* (from phylum to class) and the class *Anaerolineae* (within the phylum *Chloroflexi*). Additionally, *Spirochaetota* (from phylum to class) is enriched for the first time, while *Acidobacteriota* is only enriched at the phylum level. Notably, in the IBP-SA (Figure 3C) cathode, a significant enrichment of *Alphaproteobacteria* (within the *Proteobacteria* phylum) is observed, along with *Actinobacteriota* (from phylum to class), *Planctomycetota* (from phylum to class), and the class *Bacilli*.

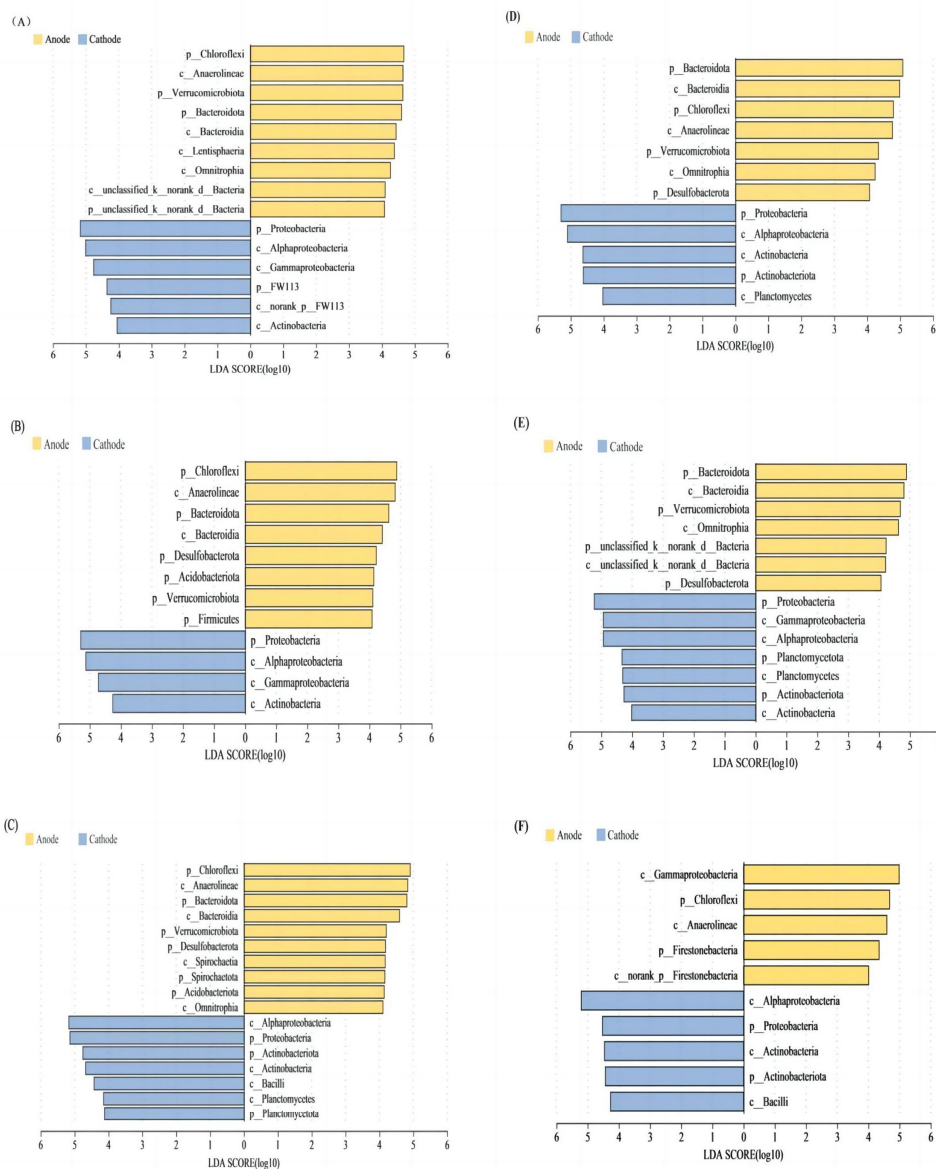


Figure 3. Indicator bacterial with LDA scores of 4 or greater in anodes and cathodes with different co-substrate combinations: (A) IBP-Glu, (B) IBP-Suc, (C) IBP-SA, (D) DCF-Glu, (E) DCF-Suc, (F) DCF-SA.

Figure 3D represents the bacterial composition of the CW-MFC anode and cathode in the DCF-Glu anode, and there is a higher occurrence of *Bacteroidota* (from phylum to class), along with enrichments of *Chloroflexi* (from phylum to class) and *Verrucomicrobiota* (from phylum to class). In the cathode, there remains a notable abundance of *Alphaproteobacteria* (within the *Proteobacteria* phylum), alongside enrichments of *Actinobacteriota* (from phylum

to class) and the *Planctomycetota* phylum. Moving to DCF-Suc (Figure 3E), the anode is enriched with *Bacteroidota* (from phylum to class), *Omnitrophia* (within *Verrucomicrobiota*), and *Desulfobacterota* at the phylum level. In the cathode of DCF-Suc, *Proteobacteria* (including the classes *Alphaproteobacteria* and *Gammaproteobacteria*) are predominant, which is similar to the patterns observed in IBP-Glu (Figure 3A) and IBP-Suc (Figure 3B). However, the DCF-Suc cathode exhibits a higher proportion of *Planctomycetota* (from phylum to class) compared to the IBP groups. In DCF-SA (Figure 3F), the anode is enriched with a significant abundance of *Gammaproteobacteria* (within the phylum *Proteobacteria*), *Chloroflexi* (from phylum to class), and *Anaerolineae* (within the phylum *Chloroflexi*). It is worth noting that the phylum *Firestonebacteria* is enriched in DCF-SA. On the cathode side, *Proteobacteria* (including the class *Alphaproteobacteria*), *Actinobacteriota* (from phylum to class), and the class *Bacilli* are detected and found to be enriched.

LEfSe analysis was employed to discriminate the indicator microbial communities at various taxonomic levels, ranging from domain to class in the cathodes and anodes of three CW-MFC devices (CM-A, CM-B, and CM-C) during the removal of IBP and DCF. The selection criteria were based on an LDA score exceeding 4. In the anode treated with IBP (Figure 4A), *Bacteroidota* (from phylum to class) is enriched in CM-A. CM-B displays an enrichment of the class *Bacilli* (within the phylum *Firmicutes*), while CM-C shows a high abundance of the phylum *Spirochaetota*. When removing DCF, in the cathode (Figure 4B), the class *Alphaproteobacteria* (within phylum *Proteobacteria*) is enriched in CM-C. CM-B demonstrates a higher abundance of the class *Desulfobaccia* (within the phylum *Desulfobacterota*) and the class *Chlorobia* (within the phylum *Bacteroidota*). In the anode (Figure 4C), *Bacteroidota* (from phylum to class) is enriched in CM-A. CM-B exhibits an enrichment of the class RBG-16-55-12 (within the phylum *Actinobacteriota*), and the phylum *Patescibacteria* is also enriched.

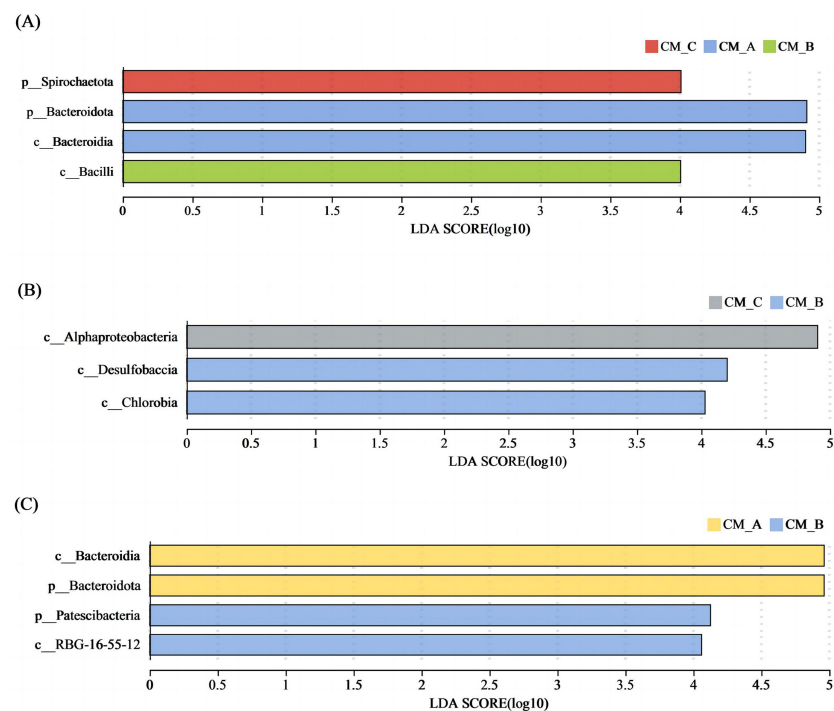


Figure 4. Indicator bacterial with LDA scores of 4 or greater in cathodes and anodes of CW-MFC devices. (A) Anode treated with IBP; (B) cathode treated with DCF; (C) anode treated with DCF.

Figure 5A,B illustrates the differences in cathodic and anodic bacterial communities among the devices of CM-A, CM-B, and CM-C when IBP is removed. PCoA analysis indicates that the influence of the co-substrates on the cathodic bacterial community is not significant. (ANOSIM, $p = 0.8400$, Figure 5A). However, significant differences emerge in the

anodic bacterial community (ANOSIM, $p = 0.0110$, Figure 5B). Furthermore, when dealing with the contaminant DCF, the co-substrates significantly affect the bacterial community structure in both the cathode (ANOSIM, $p = 0.0330$, Figure 5C) and the anode (ANOSIM, $p = 0.0200$, Figure 5D) of the CW-MFC.

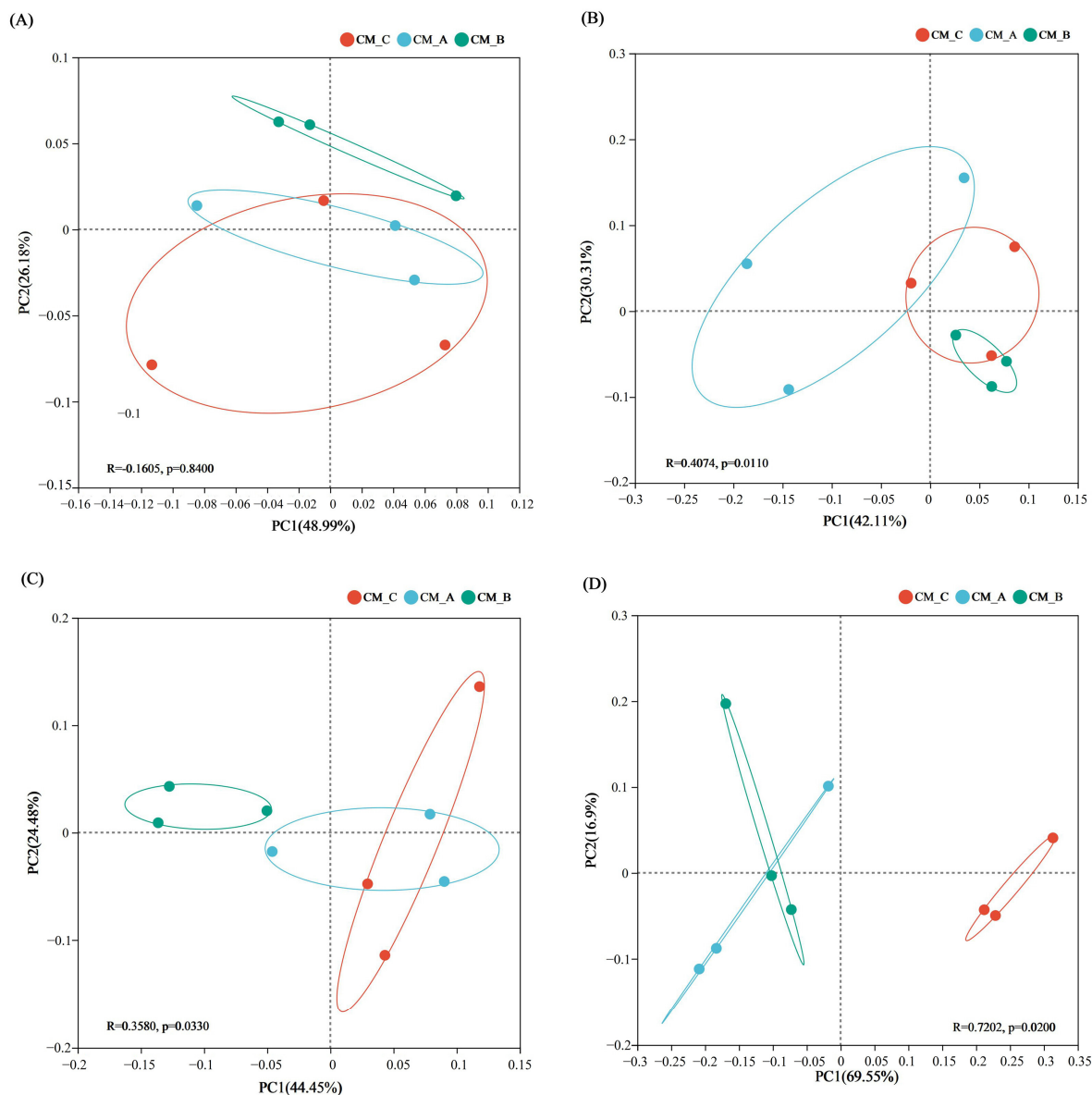


Figure 5. Principal Coordinates Analysis (PCoA) for the β -diversity between devices of CM-A, CM-B, and CM-C at the cathodes and anodes. (A) Cathode treated with IBP; (B) anode treated with IBP; (C) cathode treated with DCF; (D) anode treated with DCF.

During the IBP removal process by CW-MFC, at the family level, environmental variables (Glu, Suc, SA, $\text{NH}_4^+\text{-N}$, TN, and TP) explained 73.91% and 85.67% of the total changes in bacterial community composition at the cathode (Figure 6A) and anode (Figure 6B), respectively. In the anode, environmental variables significantly influence changes in the bacterial community ($p < 0.05$). Among the top five species in terms of abundance in the anode, the abundance of the family *Moraxellaceae* is positively correlated with the concentration of SA, while the abundance of the family *Weeksellaceae* is positively correlated with the concentration of Glu (Figure 6B).

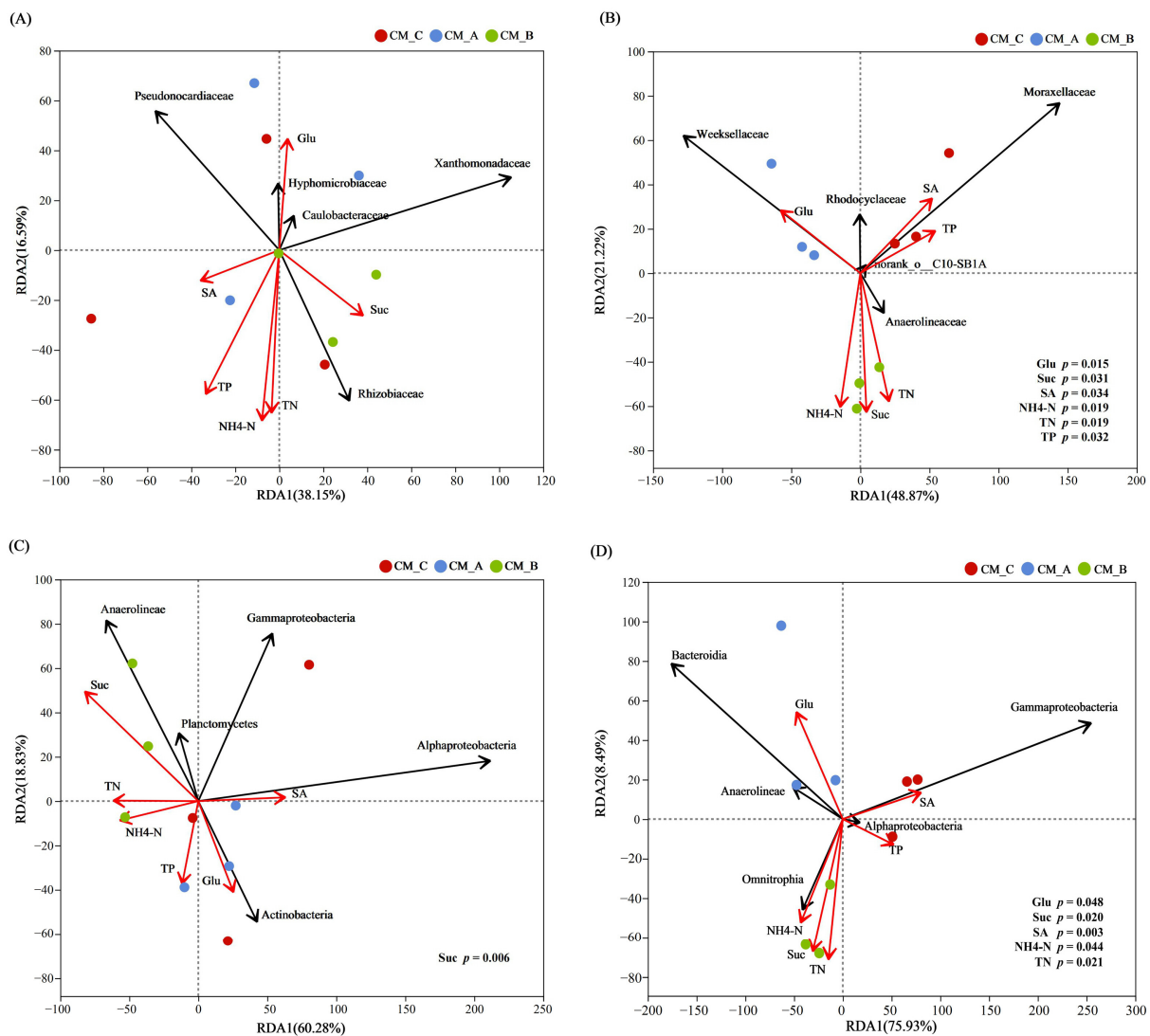


Figure 6. Redundancy analysis (RDA) between samples and environmental variables (Glu, Suc, SA, $\text{NH}_4^+\text{-N}$, TN, and TP). (A) Cathode treated with IBP; (B) Anode treated with IBP; (C) Cathode treated with DCF; (D) Anode treated with DCF.

Figure 6C,D illustrates the effects of environmental variables (Glu, Suc, SA, $\text{NH}_4^+\text{-N}$, TN, and TP) at the class level on the composition of bacterial communities in the cathode and anode during DCF removal in CW-MFC. The explainability of environmental factors on the changes in the bacterial community composition in the cathode and anode is 90.88% and 89.40%. In the cathode, changes at the class level were closely associated with Suc ($p = 0.06$, Figure 6C). In the anode, aside from TP, the other five environmental variables significantly influence the bacterial community at the class level (Figure 6D).

The correlation analysis of environmental variables (COD, $\text{NH}_4^+\text{-N}$, TN, TP, IBP, and DCF) with the bacterial community in CW-MFC cathodes at the phylum level (Figure 7A) indicates significant negative correlations. Specifically, the abundance of *Cyanobacteria*, *Firmicutes*, and *Actinobacteriota* is significantly negatively correlated with COD concentration. The abundance of *Verrucomicrobiota* is significantly negatively correlated with $\text{NH}_4^+\text{-N}$ concentration, while the abundance of *Patescibacteria* exhibits significantly negative correlation with $\text{NH}_4^+\text{-N}$, TN, and TP concentrations. The correlation analysis of environmental factors with the bacterial community at the phylum level in the anodes (Figure 7B) reveals several significant correlations. *Campilobacterota*, *Firmicutes*, *Bdellovibrionota*, *Patescibacteria*, and *Desulfobacterota* exhibit significant positive correlations with $\text{NH}_4^+\text{-N}$ concentration.

Conversely, *Campilobacterota* and *Firmicutes* are significantly negatively correlated with TP concentration. In addition, the abundance of *Actinobacteriota* and *Bacteroidota* is also significantly negatively correlated with TP concentration. It is worth noting that among the top 20 most abundant bacteria in the anode, only the abundance of *Proteobacteria* is significantly positively correlated with TP. IBP concentration is positively correlated with the abundance of most anode bacteria, including significant correlations with *Armatimonadota* and *Chloroflexi*.

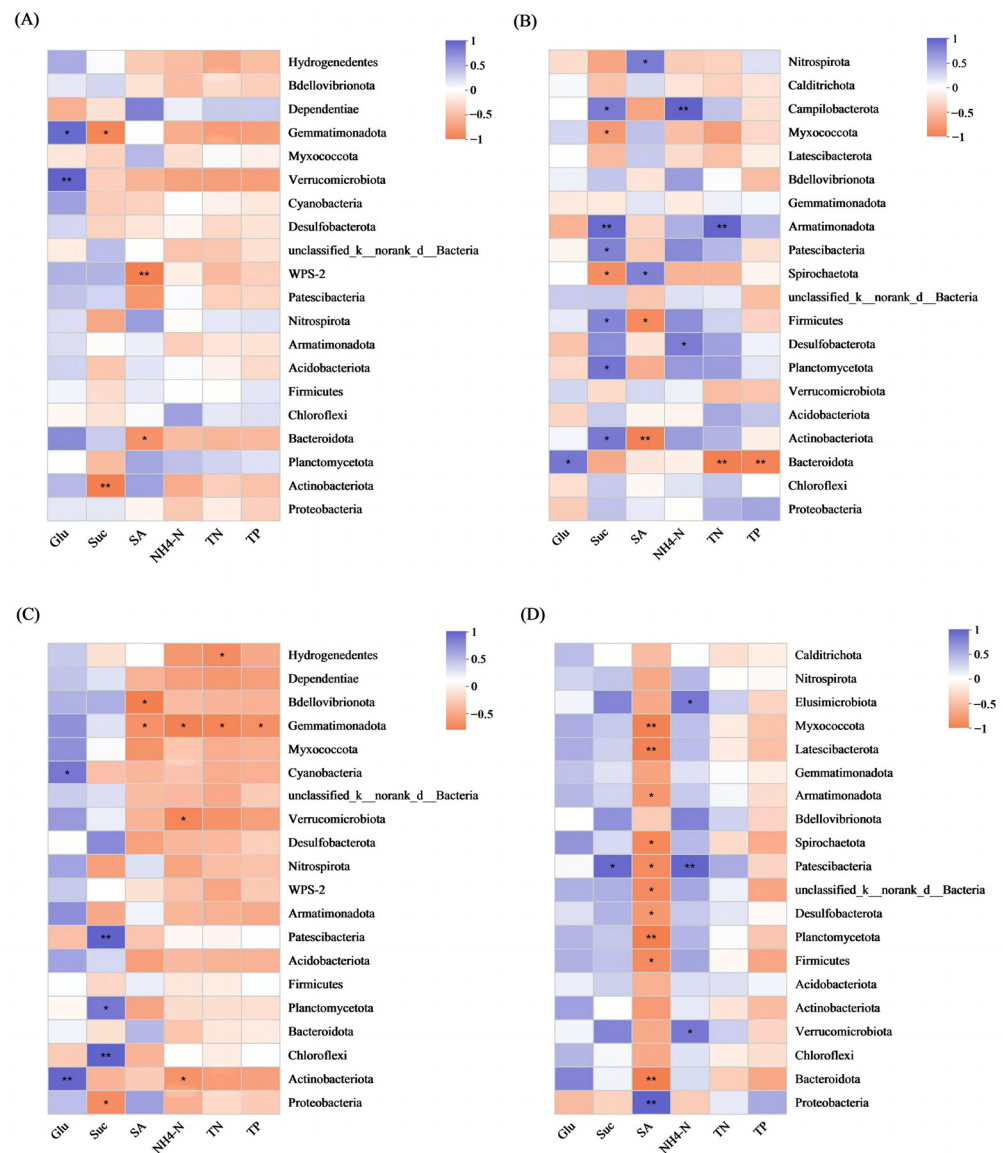


Figure 7. Correlation analysis of Glu, Suc, SA, NH₄⁺-N, TN, and TP concentrations, as well as dominant bacteria in cathodes and anodes at the phylum level. Orange indicates negative correlations, while purple indicates positive correlations. The darker the color, the stronger the correlation (* p < 0.05, ** p < 0.01). (A) Cathode treated with IBP; (B) anode treated with IBP; (C) cathode treated with DCF; (D) anode treated with DCF.

Figure 7 presents a correlation heatmap illustrating the relationships between cathode and anode bacterial communities at the phylum level with environmental variables (Glu, Suc, SA, NH₄⁺-N, TN, and TP) after PPCPs treatment. In the cathode bacterial community treated with IBP (Figure 7A), the abundance of *Gemmatimonadota* and *Verrucomicrobiota* are significantly positively correlated with Glu concentration, while the abundance of *Gemmatimonadota* is significantly negatively correlated with Suc concentra-

tion (Figure 7A). Additionally, the phylum *Actinobacteriota* shows a negative correlation with Suc concentration (Figure 7A). In the anode community treated with IBP (Figure 7B), several significant correlations are identified. The abundances of *Campilobacterota*, *Armatimonadota*, *Patescibacteria*, *Firmicutes*, *Planctomycetota*, and *Actinobacteriota* are positively correlated with Suc concentration. SA concentration shows positive correlations with the abundances of *Spirochaetota* and *Nitrospirota* but is negatively correlated with *Firmicutes* and *Actinobacteriota*. Glu concentration is only significantly positively correlated with *Bacteroidota*, while the abundance of *Bacteroidota* is negatively correlated with TN and TP concentrations (Figure 7B).

In the cathode bacterial community after DCF treatment (Figure 7C), the phylum *Actinobacteriota* is significantly positively correlated with Glu but is negatively correlated with $\text{NH}_4^+\text{-N}$ concentration. The abundance of *Gemmatimonadota* is negatively correlated with SA, $\text{NH}_4^+\text{-N}$, TN, and TP concentrations, while it exhibits a positive correlation with Glu, although not significantly (Figure 7C). In the anode community after DCF treatment (Figure 7D), the abundance of *Elusimicrobiota* phylum is positively correlated with $\text{NH}_4^+\text{-N}$ and Suc concentrations. Ten phyla, including *Myxococcota* and *Armatimonadota*, are significantly negatively correlated with SA concentration, while the abundance of *Proteobacteria* is significantly positively correlated with SA concentration. Additionally, the abundance of *Patescibacteria* phylum is significantly positively correlated with Suc and $\text{NH}_4^+\text{-N}$ concentrations (Figure 7D).

3.3. Nutrient Removal with Different Carbon Sources

After continuous operation for 60 days, the removal of COD, $\text{NH}_4^+\text{-N}$, TN, and TP in devices of CM-A, CM-B, and CM-C is depicted in Table 4. At sampling port 4, the COD concentration in CM-C was $119.10 \pm 0.70 \text{ mg L}^{-1}$, significantly differing from CM-A ($175.40 \pm 2.29 \text{ mg L}^{-1}$) and CM-B ($170.70 \pm 2.29 \text{ mg L}^{-1}$) ($p < 0.05$; Table 4). Conversely, at sampling port 5, sampling port 10, and the effluent, significantly higher COD detection concentrations were observed in CM-B compared to the other two groups of devices ($p < 0.05$; Table 4). In the end, the device of CM-A exhibited the highest average COD removal amount, removing $280.06 \pm 6.98 \text{ mg L}^{-1}$ of COD. Following that, CM-C removed $274.73 \pm 2.27 \text{ mg L}^{-1}$ of COD, while CM-B displayed the lowest COD removal of only $256.54 \pm 1.73 \text{ mg L}^{-1}$ (with the initial concentration of COD being 300 mg L^{-1}).

Table 4. Concentrations of COD, $\text{NH}_4^+\text{-N}$, TN, and TP of sampling ports and effluent using different carbon sources. Uppercase and lowercase letters represent intra-group and inter-group differences, respectively. Different letters indicate significant differences, with $p < 0.05$ (mean \pm SD, $n = 3$).

Pollutants	Samples	Concentration ($\text{mg}\cdot\text{L}^{-1}$)				
		Sampling Port 4	Sampling Port 5	Sampling Port 10	Effluent	Total Removal
COD	CM-A	175.40 ± 2.29 ^{Aa}	42.33 ± 7.22 ^{Bb}	25.36 ± 6.69 ^{Cb}	19.94 ± 6.98 ^{Ca}	280.06 ± 6.98 ^a
	CM-B	170.70 ± 2.29 ^{Ab}	64.92 ± 2.17 ^{Ba}	47.48 ± 1.78 ^{Ca}	43.46 ± 1.73 ^{Db}	256.54 ± 1.73 ^b
	CM-C	119.10 ± 0.70 ^{Ac}	42.83 ± 2.00 ^{Bb}	27.02 ± 2.22 ^{Cb}	25.27 ± 2.27 ^{Cb}	274.73 ± 2.27 ^a
$\text{NH}_4^+\text{-N}$	CM-A	23.61 ± 0.01 ^{Aa}	17.30 ± 0.01 ^{Bb}	16.86 ± 0.01 ^{Cb}	9.60 ± 0.06 ^{Dc}	25.20 ± 0.06 ^a
	CM-B	22.41 ± 0.02 ^{Ab}	18.82 ± 0.01 ^{Ba}	18.55 ± 0.02 ^{Ca}	13.12 ± 0.06 ^{Db}	21.68 ± 0.06 ^b
	CM-C	18.99 ± 0.12 ^{Ac}	16.34 ± 0.13 ^{Bc}	16.25 ± 0.12 ^{Bc}	14.46 ± 0.10 ^{Ca}	20.34 ± 0.10 ^b
TN	CM-A	21.16 ± 0.01 ^{Ab}	13.42 ± 0.08 ^{Bc}	12.52 ± 0.15 ^{Cc}	3.87 ± 0.19 ^{Dc}	30.93 ± 0.19 ^a
	CM-B	22.04 ± 0.07 ^{Aa}	16.59 ± 0.00 ^{Ba}	15.97 ± 0.03 ^{Ca}	9.64 ± 0.00 ^{Db}	25.16 ± 0.00 ^b
	CM-C	18.22 ± 0.11 ^{Ac}	14.50 ± 0.04 ^{Bb}	14.02 ± 0.08 ^{Cb}	10.65 ± 0.04 ^{Da}	24.15 ± 0.04 ^c
TP	CM-A	273.09 ± 0.30 ^{Ac}	235.49 ± 0.39 ^{Bc}	189.80 ± 0.87 ^{Cc}	148.07 ± 0.39 ^{Dc}	227.93 ± 0.39 ^a
	CM-B	274.86 ± 0.33 ^{Ab}	243.06 ± 0.22 ^{Bb}	203.72 ± 0.60 ^{Cb}	163.95 ± 0.63 ^{Db}	212.05 ± 0.63 ^b
	CM-C	293.00 ± 0.30 ^{Aa}	272.91 ± 1.39 ^{Ba}	241.59 ± 0.96 ^{Ca}	213.58 ± 1.32 ^{Da}	162.42 ± 1.32 ^c

At sampling port 4, the concentration of $\text{NH}_4^+\text{-N}$ in CM-C was the lowest at $18.99 \pm 0.12 \text{ mg L}^{-1}$, whereas CM-A displayed the highest detected concentration at this location, which was $23.61 \pm 0.01 \text{ mg L}^{-1}$ ($p < 0.05$; Table 4). However, at sampling

port 5 and sampling port 10, the highest concentration of $\text{NH}_4^+\text{-N}$ was observed in CM-B ($p < 0.05$; Table 4). In the final effluent, the highest concentration was observed in the device of CM-C, at $14.46 \pm 0.10 \text{ mg L}^{-1}$ ($p < 0.05$; Table 4). On average, the devices of CM-A exhibited the highest $\text{NH}_4^+\text{-N}$ removal of $25.20 \pm 0.06 \text{ mg L}^{-1}$, significantly higher than that in CM-B ($21.68 \pm 0.06 \text{ mg L}^{-1}$) and CM-C ($20.34 \pm 0.10 \text{ mg L}^{-1}$) ($p < 0.05$; Table 4) (with the initial concentration of $\text{NH}_4^+\text{-N}$ was 34.8 mg L^{-1}).

At sampling port 4, the TN concentration in CM-C was the lowest, measuring $18.22 \pm 0.11 \text{ mg L}^{-1}$. Conversely, CM-B recorded the highest detected concentration at $22.04 \pm 0.07 \text{ mg L}^{-1}$, while CM-A showed a TN concentration of $21.16 \pm 0.01 \text{ mg L}^{-1}$ ($p < 0.05$; Table 4). At sampling ports 5 and 10, the highest TN concentrations were consistently observed in the device of CM-B ($p < 0.05$; Table 4). However, in the effluent, the highest TN concentration was noted in the device of CM-C, at $10.65 \pm 0.04 \text{ mg L}^{-1}$ ($p < 0.05$; Table 4). On average, CM-A achieved the highest TN removal, measuring $30.93 \pm 0.19 \text{ mg L}^{-1}$, significantly surpassing the TN removal amount in CM-B ($25.16 \pm 0.00 \text{ mg L}^{-1}$) and CM-C ($24.15 \pm 0.04 \text{ mg L}^{-1}$) ($p < 0.05$; Table 4) (with an initial TN concentration of 34.8 mg L^{-1}).

At sampling port 4, CM-A exhibited the lowest average TP concentration at $273.09 \pm 0.30 \text{ mg L}^{-1}$, while CM-B had a concentration of $274.86 \pm 0.33 \text{ mg L}^{-1}$ and CM-C showed the highest average TP concentration, reaching $293.00 \pm 0.30 \text{ mg L}^{-1}$ (Table 4). Significant differences in TP concentrations were observed among these devices ($p < 0.05$). It is noteworthy that the relative magnitudes and differences in average TP concentrations among the three devices remained consistent at sampling ports 5 and 10 and the effluent. Consequently, devices of CM-A achieved the highest average TP removal, of $227.93 \pm 0.39 \text{ mg L}^{-1}$, followed by CM-B, with $212.05 \pm 0.63 \text{ mg L}^{-1}$, while CM-C had the lowest average TP removal, at only $162.42 \pm 1.32 \text{ mg L}^{-1}$ ($p < 0.05$; Table 4) (with an initial TP concentration of 376 mg L^{-1}).

3.4. The Electrical Characteristics of CW-MFCs

Figures 8 and 9 display DO variation over height in CW-MFC and the polarization and power density curves of the CW-MFC under the influence of different carbon sources. The polarization curves on the left axis all exhibit good fits, indicating stable electricity generation performance for the CW-MFC devices using the three different carbon sources. The highest point on the power density curve on the right axis represents the maximum power density, denoted as P_{max} . In this study, the CW-MFC with Glu as the carbon source exhibited a P_{max} (maximum power output) of 75.50 mW/m^3 , significantly higher than that of CW-MFCs with SA or Suc as the co-substrates.

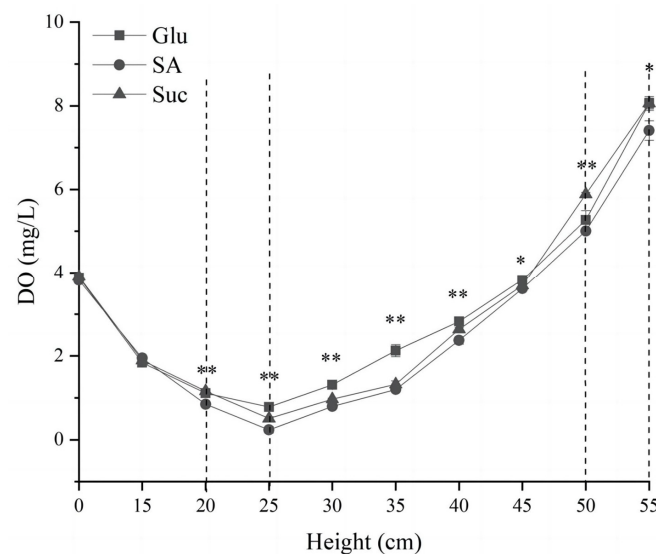


Figure 8. DO variation over height in CW-MFC. * indicate significant differences, with * $p < 0.05$, ** $p < 0.01$.

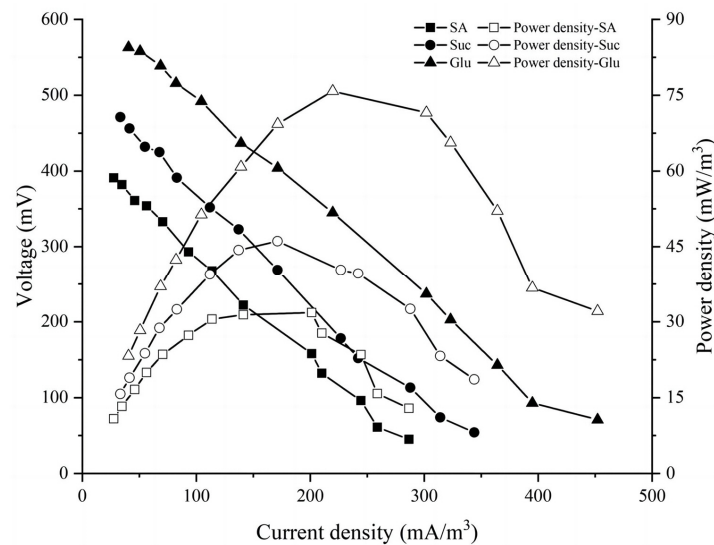


Figure 9. Polarization curve and power density curve with different carbon sources.

4. Discussion

4.1. Effects of Different Co-Substrates on PPCP Removal

When Glu is used as a co-substrate, the total removal of IBP is significantly higher compared to Suc and SA as co-substrates. Specifically, in the CM-A anode region (between sampling points 4 and 5), the removal rate of IBP is notably higher than in the bottom layer (between influent and sampling point 4), middle layer (between sampling points 5 and 10), and the cathode layer (between sampling point 10 and effluent) (Table 1). Similar observations are also made in CM-B and CM-C. Regarding the removal of DCF, when Glu and Suc are used as co-substrates, the CW-MFC significantly removes a higher total amount of DCF compared to SA as the co-substrate. Primary removal of DCF predominantly occurs in the anode and the bottom layer, with significant differences observed among various co-substrates ($p < 0.05$, Table 2). It is evident that CW-MFC's efficiency in removing both IBP and DCF is closely associated with the anode, which exhibits higher microbial biomass and diversity compared to the cathode (Table 3). These findings align with numerous research results highlighting the pivotal role of microorganisms enriched in the anode in the transformation and utilization of PPCPs [59,60]. In this study, the bottom layer and middle layer show relatively high removal rates for DCF. However, different co-substrates do not significantly affect the removal of DCF in the middle layer ($p > 0.05$, Table S2). The composition of the middle layer is gravel, with a volume of 6.28 L. Gravel is a common material for CW and CW-MFC construction. Some researchers used the gravel bed CW to remove ten types of PPCPs and identified the presence of 4-hydroxy-diclofenac in the pore water and effluent [54], which is a common transformation product of DCF in wastewater [61]. This suggests that biodegradation in CW pore water is also one of the removal pathways for DCF. However, the transformation of DCF in CW-MFC still needs more research. Overall, the CW-MFC device constructed in this study exhibits relatively good removal performance for both IBP and DCF (Tables 1 and 2), surpassing the results reported in previous research studies [31]. Both Glu and Suc as co-substrates outperform SA in PPCP removal. In CM-C, the Sobs and Shannon indices in the cathode and anode are significantly lower than in CM-A and CM-B (Table 3). SA has a smaller molecular weight (82.03) and a simpler structure, which results in faster consumption in the bottom and anode layers, leading to a carbon source deficiency in the cathode. This explains why the CM-C device has lower PPCP concentrations at sampling port 4, which is closest to the influent, but the lowest overall PPCP removal.

4.2. Effects of Different Co-Substrates on Bacterial Community

The electrodes are considered the primary locations for microbial enrichment and hold significant importance in the CW-MFC system for both pollutant removal and electricity generation [31,62,63]. In this study, phyla such as *Firmicutes*, *Actinobacteria*, and *Acidobacteria* (Figure 3) found in the anode have been identified as EAB [64]. These bacteria not only participate in electricity generation but are also believed to play a crucial role in enhancing the diversity of the bacterial community (Figure 4) [65,66]. Furthermore, in the study, when Glu and Sucrose Suc were co-metabolized with the two PPCPs, both resulted in an enrichment of *Bacteroidota* in the anodic bacterial community (Figure 3A,B,D,E). However, this dominance was not observed with DCF-SA (Figure 3F). *Bacteroidota* is a dominant group in anaerobic granular sludge (AGS) [67], suggesting that their source may be seeded AGS. This phenomenon suggests that the simulated wastewater used in this study had an appropriate organic concentration, meeting the metabolic activity requirements of the seeded AGS. In the case of the DCF-SA combination, SA was used for electricity generation, resulting in insufficient organic concentration at the anode. Likewise, the enrichment of *Planctomycetota* was observed in the cathodes of various co-substrate combinations (Figure 3), but it was somewhat inhibited in the DCF-SA cathode (Figure 3F). *Planctomycetota* are involved in various biogeochemical cycles in river ecosystems, encompassing element redox reactions, pollutant degradation, nitrogen cycling, and carbon utilization [68]. This observation may account for the lower removal rate of TN by DCF (Table 4).

In this study, the choice of co-substrate significantly influences the bacterial community composition in the CW-MFC anode during IBP treatment, while it does not significantly affect the cathode bacterial composition (Figure 5A). Additionally, the family *Weeksellaceae* (within the phylum *Bacteroidota*) in the anode, after IBP treatment, is significantly positively correlated with the concentration of Glu (Figures 6B and 7B), yet it is absent in the cathode. The genus *Chryseobacterium*, which falls within the family *Weeksellaceae*, is known to be involved in the degradation of various exogenous drugs, including fungicides like Mancozeb [69] and herbicides [70]. This suggests that the *Weeksellaceae* family may be responsible for the primary biodegradation of IBP. Furthermore, in the IBP-treated anode, the family *Moraxellaceae* demonstrates a significant positive correlation with SA concentration (Figure 6B). *Moraxellaceae*, a family of *Gammaproteobacteria*, includes the genus *Moraxella*, which is known for its ability to thrive using unstable compounds, particularly dissolved organic matter [71]. Moreover, *Gammaproteobacteria* are commonly employed as EAB in MFC systems [72]. In the IBP-treated anode, Suc is positively correlated with *Anaerolineaceae* (Figure 6B), which belongs to the *Chloroflexi* phylum. Microorganisms within the *Anaerolineaceae* family are often associated with anaerobic ammonia oxidation processes, suggesting their capacity to utilize organic carbon generated from cell lysis for growth [73,74]. Furthermore, in the IBP-treated anode, the correlation of Suc and $\text{NH}_4^+\text{-N}$ with various bacteria is consistent (Figure 7B). This suggests that Suc, compared to Glu, is less readily metabolized by microorganisms, allowing it to be more involved in anaerobic ammonia oxidation processes [75].

The choice of co-substrate significantly influences both the cathode and anode bacterial communities during DCF treatment (Figure 5C,D). In the cathode bacterial community during DCF treatment, the variation is primarily dependent on Suc concentration (Figure 6C). This can be attributed to the fact that Suc needs to undergo hydrolyzation before it becomes accessible for microbial utilization, rendering it more likely to be a source of carbon for cathode bacteria.

In the cathode bacterial community during DCF treatment, *Patescibacteria*, *Planctomycetota*, and *Chloroflexi* are significantly positively correlated with Suc concentration (Figures 4C and 7C). *Chloroflexi* and *Planctomycetes* are known for their potential involvement in the removal of PPCPs [76]. While the gravel fillers in the device possess some adsorption capacity for DCF, as the experiment progresses and the adsorption reaches saturation, the concentration of DCF not degraded by anodic bacteria gradually increases and flows toward the cathode. This could provide an opportunity for the enrichment of *Chlo-*

roflexi and *Planctomycetes* in the cathode (Figure 7C). Previous research has shown that the addition of PPCPs to bioreactors can promote the dominance of *Proteobacteria* [77]. This may explain the phenomenon in Figure 7D, where SA is significantly positively correlated only with the *Proteobacteria* phylum. The easily utilizable SA co-substrate is rapidly consumed by *Proteobacteria* upon entering the anode during DCF treatment, further contributing to its dominance.

4.3. Effect of Different Co-Substrates on the CW-MFC Performance

The COD removal rate in CW-MFC is influenced by various factors, including device configuration, initial COD concentration, HRT, wastewater characteristics, and bacterial communities [78]. In this study, the COD removal rate in CW-MFC exceeded that reported in previous research with similar configurations [79,80]. Previous studies have suggested that the higher COD removal rate of CW-MFC compared to CWs is due to the introduction of electrodes and conductive materials. Conductive materials can use themselves as temporary electron acceptors to accelerate the anaerobic oxidation process of pollutants [81]. Higher bacterial community diversity in the anode also promotes COD removal (Table 3). For example, GAC, the electrode material in this study, possesses the capability to extract electrons from organic compounds, enhancing the attachment of bacteria to GAC particles within the anode layer [82]. In addition, the COD adsorption behaviors of gravel cannot be ignored. Depending on the initial concentration and loading amount, the COD removal efficiency of gravel is in the range of 18.76~38.15% [83].

The removal of $\text{NH}_4^+\text{-N}$ in CW-MFC systems is believed to primarily depend on nitrification in the presence of oxygen. Therefore, the residual carbon source content available to drive the nitrification reaction in the cathode and the cathode's structure characteristics are critical factors in the nitrogen removal in CW-MFC [84]. In this study, the DO concentration is depicted in Figure 8, showing that the DO brought in with the influent and cathode is higher than other locations of the system. The removal patterns for $\text{NH}_4^+\text{-N}$ and TN also exhibit higher removal rates in the bottom layer and cathode in comparison to other layers. As SA is the most readily decomposed carbon source, it supplies the smallest amount of carbon at the cathode, resulting in the lowest removal rates for $\text{NH}_4^+\text{-N}$ and TN in CW-MFC when SA is used as the carbon source. These findings are consistent with previous research [85]. However, some researchers believe that the overall effective denitrification performance in CW-MFC is mainly attributed to the diverse bacterial communities and the presence of abundant electroactive bacteria, which contribute to enhancing the rates of anaerobic ammonium oxidation, nitrification, and denitrification processes within CW-MFC [31,66,86].

Regarding the removal of TP, Glu is a more suitable carbon source compared to SA and Suc. TP removal is the greatest (Table 4), and the removal rate is 60.62%, lower than reported in previous research [87,88]. Typically, phosphorus compounds are removed in CW-MFC through biological or physicochemical processes. Some researchers argue that physicochemical processes play a more substantial role in TP removal than biological processes [38,89]. We found that only the bacterial community composition in the IBP-treated anode was significantly affected by TP concentration, and biodegradation made a limited contribution to TP removal (Figure 6). Some researchers have even observed unexplained reductions in TP removal rates in conventional CWs coupled with MFC [90]. Therefore, further research on plant species, system configuration, and microbial communities is essential to enhance our comprehension of the elements influencing reduced rates of TP removal.

SA is typically recognized as a carbon source that stimulates the proliferation of electroactive bacteria (Figure 6) [49]. However, in this study, when SA was used as the co-substrate, the CW-MFC exhibited the lowest output voltage and device power density, while the Glu co-substrate showed the best electricity generation performance (Figure 9), which is similar to findings reported in previous studies [57,91]. This difference can be attributed to the fact that Glu participates more rapidly in the electricity-producing process

compared to SA, generating higher electrical energy in a shorter time. However, over prolonged operation, SA as the co-substrate might lead to a decrease in microbial diversity within the CW-MFC [92]. Additionally, the SA co-substrate undergoes electrochemical reactions that generate acids under anaerobic conditions. This acid production reduces the pH of the anode environment and inhibits the activity of anaerobic microorganisms, consequently reducing the system's electricity generation performance [93]. On the other hand, the Glu co-substrate may result in electron competition among bacteria. Nevertheless, a more diverse bacterial composition is advantageous for the degradation of complex substrates [94].

This study focuses on how different carbon sources affect the co-metabolic removal of PPCPs, therefore maintaining a relatively conservative approach to device design, electrode selection, and operating conditions of the CW-MFC system. In the future, more research is needed for more efficient removal of PPCPs from wastewater by CW-MFC. For instance, optimizing the HRT can potentially achieve IBP removal rates exceeding 95% due to its simple structure [31]. Additionally, exploring the utilization of new functional complexes with enhanced PPCP adsorption capabilities as electrodes or additives could significantly improve pollutant removal efficiency. Moreover, the potential application of CW-MFC as a biosensor within the CW environment holds promise for various environmental monitoring purposes [95,96].

5. Conclusions

In this study, the CW-MFC achieved high removal efficiencies of 89.29% for IBP and 84.10% for DCF, with Glu as the most effective co-substrate for PPCP removal and electricity generation. The co-metabolism of IBP and a carbon source took place in both the anode and cathode of the CW-MFC, while the co-metabolism of DCF and a carbon source primarily occurred at the anode. Furthermore, the composition of the bacterial community in the anode of IBP-treated CW-MFC was influenced by the choice of co-substrates. In contrast, the composition of the bacterial community in both the cathode and anode of DCF-treated CW-MFC was influenced by the co-substrate used. Analysis of the electrode microbial community structure revealed that the presence of SA as a co-substrate favored the induction and enrichment of EAB in the anodes within the CW-MFC. In conclusion, it is evident that CW-MFC holds significant research potential in power generation and has the capacity for larger-scale applications.

Supplementary Materials: The following supporting information can be downloaded at: <https://www.mdpi.com/article/10.3390/w15213862/s1>, Figure S1: The standard curves for IBP and DCF; Table S1: Target PPCPs used in this study and their properties; Table S2: DCF removal rates (%) of each layers.

Author Contributions: G.Q.: Conceptualization, methodology, formal analysis, data curation, writing—original draft. H.F.: formal analysis, methodology, writing—original draft. R.Y., F.Z. and X.J.: resources, investigation. L.X.: supervision, writing—review and editing. S.A.: supervision, conceptualization, resources, project administration, and funding acquisition. All authors have read and agreed to the published version of the manuscript.

Funding: This study was funded by Chaohu Basin Mountains, Waters, Forests, Fields, Lakes and Grassland Monitoring System Construction Project (Survey and Assessment Part) [2022BFAWZ02436], Research and demonstration of bird-friendly constructed wetland technology for treating aquaculture tailwater at heritage sites [HSDKT202310] and The Major Science and Technology Program for Water Pollution Control and Treatment of China [2017ZX07401003-02].

Data Availability Statement: The data are available from the corresponding author upon reasonable request.

Acknowledgments: We would like to thank Miao Zhang and Jing Chen for their assistance in the maintenance of the systems.

Conflicts of Interest: The authors declare that the research was conducted in the absence of any commercial or financial relationships that could be construed as a potential conflict of interest.

References

1. Ordóñez, C.; Pamela, D. *Determination of HPLC/MS/MS Capabilities for the Monitoring of Trace Level Pharmaceuticals and Personal Care Products (PPCP) in Environmental Samples*; California State University: Fresno, CA, USA, 2015.
2. Daughton, C.G.; Ternes, T.A. Pharmaceuticals and personal care products in the environment: Agents of subtle change? *Env. Health Perspect* **1999**, *107* (Suppl. 6), 907–938. [[CrossRef](#)] [[PubMed](#)]
3. Guruge, K.S.; Goswami, P.; Tanoue, R.; Nomiyama, K.; Wijesekara, R.G.S.; Dharmaratne, T.S. First nationwide investigation and environmental risk assessment of 72 pharmaceuticals and personal care products from Sri Lankan surface waterways. *Sci. Total Environ.* **2019**, *690*, 683–695. [[CrossRef](#)] [[PubMed](#)]
4. Ren, B.; Shi, X.; Jin, X.; Wang, X.C.; Jin, P. Comprehensive evaluation of pharmaceuticals and personal care products (PPCPs) in urban sewers: Degradation, intermediate products and environmental risk. *Chem. Eng. J.* **2021**, *404*, 127024. [[CrossRef](#)]
5. Yang, H.; Lu, G.; Yan, Z.; Liu, J.; Dong, H.; Jiang, R.; Zhou, R.; Zhang, P.; Sun, Y.; Nkoom, M. Occurrence, spatial-temporal distribution and ecological risks of pharmaceuticals and personal care products response to water diversion across the rivers in Nanjing, China. *Environ. Pollut.* **2019**, *255*, 113132. [[CrossRef](#)] [[PubMed](#)]
6. Menger, F.; Ahrens, L.; Wiberg, K.; Gago-Ferrero, P. Suspect screening based on market data of polar halogenated micropollutants in river water affected by wastewater. *J. Hazard. Mater.* **2021**, *401*, 123377. [[CrossRef](#)] [[PubMed](#)]
7. Rainsford, K.D. Ibuprofen: Pharmacology, efficacy and safety. *Inflammopharmacology* **2009**, *17*, 275–342. [[CrossRef](#)]
8. Zhao, J.-L.; Ying, G.-G.; Wang, L.; Yang, J.-F.; Yang, X.-B.; Yang, L.-H.; Li, X. Determination of phenolic endocrine disrupting chemicals and acidic pharmaceuticals in surface water of the Pearl Rivers in South China by gas chromatography–negative chemical ionization–mass spectrometry. *Sci. Total Environ.* **2009**, *407*, 962–974. [[CrossRef](#)]
9. Bu, Q.W.; Wang, B.; Huang, J.; Deng, S.B.; Yu, G. Pharmaceuticals and personal care products in the aquatic environment in China: A review. *J. Hazard. Mater.* **2013**, *262*, 189–211. [[CrossRef](#)]
10. Evgenidou, E.N.; Konstantinou, I.K.; Lambropoulou, D.A. Occurrence and removal of transformation products of PPCPs and illicit drugs in wastewaters: A review. *Sci. Total Environ.* **2015**, *505*, 905–926. [[CrossRef](#)]
11. Mei, X.; Sui, Q.; Lyu, S.; Wang, D.; Zhao, W. Pharmaceuticals and personal care products in the urban river across the megacity Shanghai: Occurrence, source apportionment and a snapshot of influence of rainfall. *J. Hazard. Mater.* **2018**, *359*, 429–436. [[CrossRef](#)]
12. Jia, Y.; Yin, L.; Khanal, S.K.; Zhang, H.; Oberoi, A.S.; Lu, H. Biotransformation of ibuprofen in biological sludge systems: Investigation of performance and mechanisms. *Water Res.* **2020**, *170*, 115303. [[CrossRef](#)] [[PubMed](#)]
13. Al-Qaim, F.F.; Abdullah, M.P.; Othman, M.R.; Latip, J.; Zakaria, Z. Multi-residue analytical methodology-based liquid chromatography-time-of-flight-mass spectrometry for the analysis of pharmaceutical residues in surface water and effluents from sewage treatment plants and hospitals. *J. Chromatogr. A* **2014**, *1345*, 139–153. [[CrossRef](#)] [[PubMed](#)]
14. Zhang, Y.; Geißen, S.-U.; Gal, C. Carbamazepine and diclofenac: Removal in wastewater treatment plants and occurrence in water bodies. *Chemosphere* **2008**, *73*, 1151–1161. [[CrossRef](#)] [[PubMed](#)]
15. Landsorp, D.; Vree, T.B.; Janssen, T.J.; Guelen, P.J. Pharmacokinetics of rectal diclofenac and its hydroxy metabolites in man. *Int. J. Clin. Pharmacol. Ther. Toxicol.* **1990**, *28*, 298–302.
16. Heberer, T.; Feldmann, D. Contribution of effluents from hospitals and private households to the total loads of diclofenac and carbamazepine in municipal sewage effluents—modeling versus measurements. *J. Hazard. Mater.* **2005**, *122*, 211–218. [[CrossRef](#)]
17. Minella, M.; Bertinetti, S.; Hanna, K.; Minero, C.; Vione, D. Degradation of ibuprofen and phenol with a Fenton-like process triggered by zero-valent iron (ZVI-Fenton). *Environ. Res.* **2019**, *179*, 108750. [[CrossRef](#)]
18. Leverrier-Penna, S.; Mitchell, R.T.; Becker, E.; Lecante, L.; Ben Maamar, M.; Homer, N.; Lavoué, V.; Kristensen, D.M.; Dejuq-Rainsford, N.; Jégou, B.; et al. Ibuprofen is deleterious for the development of first trimester human fetal ovary ex vivo. *Hum. Reprod.* **2018**, *33*, 482–493. [[CrossRef](#)]
19. Oaks, J.L.; Gilbert, M.; Virani, M.Z.; Watson, R.T.; Meteyer, C.U.; Rideout, B.A.; Shivaprasad, H.L.; Ahmed, S.; Iqbal Chaudhry, M.J.; Arshad, M.; et al. Diclofenac residues as the cause of vulture population decline in Pakistan. *Nature* **2004**, *427*, 630–633. [[CrossRef](#)]
20. Brozinski, J.M.; Lahti, M.; Meierjohann, A.; Oikari, A.; Kronberg, L. The anti-inflammatory drugs diclofenac, naproxen and ibuprofen are found in the bile of wild fish caught downstream of a wastewater treatment plant. *Env. Sci Technol* **2013**, *47*, 342–348. [[CrossRef](#)]
21. Zheng, M.; Chen, J.; Zhang, L.; Cheng, Y.; Lu, C.; Liu, Y.; Singh, A.; Trivedi, M.; Kumar, A.; Liu, J. Metal organic frameworks as efficient adsorbents for drugs from wastewater. *Mater. Today Commun.* **2022**, *31*, 103514. [[CrossRef](#)]
22. Yadav, A.K.; Dash, P.; Mohanty, A.; Abbassi, R.; Mishra, B.K. Performance assessment of innovative constructed wetland-microbial fuel cell for electricity production and dye removal. *Ecol. Eng.* **2012**, *47*, 126–131. [[CrossRef](#)]
23. Vymazal, J.; Zhao, Y.; Mander, Ü. Recent research challenges in constructed wetlands for wastewater treatment: A review. *Ecol. Eng.* **2021**, *169*, 106318. [[CrossRef](#)]
24. Doherty, L.; Zhao, Y. Operating a two-stage microbial fuel cell-constructed wetland for fuller wastewater treatment and more efficient electricity generation. *Water Sci. Technol. A J. Int. Assoc. Water Pollut. Res.* **2015**, *72*, 421–428. [[CrossRef](#)] [[PubMed](#)]
25. Healy, M.G.; Rodgers, M.; Mulqueen, J. Treatment of dairy wastewater using constructed wetlands and intermittent sand filters. *Bioresour. Technol.* **2007**, *98*, 2268–2281. [[CrossRef](#)]

26. Patil, R.; Zahid, M.; Govindwar, S.; Khandare, R.; Vyavahare, G.; Gurav, R.; Desai, N.; Pandit, S.; Jadhav, J. Chapter 8—Constructed wetland: A promising technology for the treatment of hazardous textile dyes and effluent. In *Development in Wastewater Treatment Research and Processes*; Shah, M., Rodriguez-Couto, S., Biswas, J., Eds.; Elsevier: Amsterdam, The Netherlands, 2022; pp. 173–198.
27. Sudarsan, J.S.; Annadurai, R.; Mukhopadhyay, M.; Chakraborty, P.; Nithiyantham, S. Domestic wastewater treatment using constructed wetland: An efficient and alternative way. *Sustain. Water Resour. Manag.* **2018**, *4*, 781–787. [[CrossRef](#)]
28. Vymazal, J. Constructed wetlands for treatment of industrial wastewaters: A review. *Ecol. Eng.* **2014**, *73*, 724–751. [[CrossRef](#)]
29. Reyes-Contreras, C.; Matamoros, V.; Ruiz, I.; Soto, M.; Bayona, J.M. Evaluation of PPCPs removal in a combined anaerobic digester-constructed wetland pilot plant treating urban wastewater. *Chemosphere* **2011**, *84*, 1200–1207. [[CrossRef](#)]
30. Hartl, M.; García-Galán, M.J.; Matamoros, V.; Fernández-Gatell, M.; Rousseau, D.P.L.; Du Laing, G.; Garfí, M.; Puigagut, J. Constructed wetlands operated as bioelectrochemical systems for the removal of organic micropollutants. *Chemosphere* **2021**, *271*, 129593. [[CrossRef](#)]
31. Li, H.; Zhang, S.; Yang, X.-L.; Yang, Y.-L.; Xu, H.; Li, X.-N.; Song, H.-L. Enhanced degradation of bisphenol A and ibuprofen by an up-flow microbial fuel cell-coupled constructed wetland and analysis of bacterial community structure. *Chemosphere* **2019**, *217*, 599–608. [[CrossRef](#)]
32. Wang, J.; Wang, S. Removal of pharmaceuticals and personal care products (PPCPs) from wastewater: A review. *J. Environ. Manag.* **2016**, *182*, 620–640. [[CrossRef](#)]
33. Oon, Y.-L.; Ong, S.-A.; Ho, L.-N.; Wong, Y.-S.; Oon, Y.-S.; Lehl, H.K.; Thung, W.-E. Hybrid system up-flow constructed wetland integrated with microbial fuel cell for simultaneous wastewater treatment and electricity generation. *Bioresour. Technol.* **2015**, *186*, 270–275. [[CrossRef](#)] [[PubMed](#)]
34. Doherty, L.; Zhao, Y.; Zhao, X.; Hu, Y.; Hao, X.; Xu, L.; Liu, R. A review of a recently emerged technology: Constructed wetland – Microbial fuel cells. *Water Res.* **2015**, *85*, 38–45. [[CrossRef](#)] [[PubMed](#)]
35. Kadlec, R.H. Comparison of free water and horizontal subsurface treatment wetlands. *Ecol. Eng.* **2009**, *35*, 159–174. [[CrossRef](#)]
36. Zhu, M.; Zhang, M.; Yuan, Y.; Zhang, P.; Du, S.; Ya, T.; Chen, D.; Wang, X.; Zhang, T. Responses of microbial communities and their interactions to ibuprofen in a bio-electrochemical system. *J. Environ. Manag.* **2021**, *289*, 112473. [[CrossRef](#)]
37. Dai, M.; Zhang, Y.; Wu, Y.; Sun, R.; Zong, W.; Kong, Q. Mechanism involved in the treatment of sulfamethoxazole in wastewater using a constructed wetland microbial fuel cell system. *J. Environ. Chem. Eng.* **2021**, *9*, 106193. [[CrossRef](#)]
38. Ge, X.Y.; Cao, X.; Song, X.S.; Wang, Y.H.; Si, Z.H.; Zhao, Y.F.; Wang, W.T.; Tesfahunegn, A.A. Bioenergy generation and simultaneous nitrate and phosphorus removal in a pyrite-based constructed wetland-microbial fuel cell. *Bioresour. Technol.* **2020**, *296*, 10. [[CrossRef](#)]
39. Liu, X.; Guo, X.; Liu, Y.; Lu, S.; Xi, B.; Zhang, J.; Wang, Z.; Bi, B. A review on removing antibiotics and antibiotic resistance genes from wastewater by constructed wetlands: Performance and microbial response. *Environ. Pollut.* **2019**, *254*, 112996. [[CrossRef](#)]
40. Pan, M.; Chu, L.M. Adsorption and degradation of five selected antibiotics in agricultural soil. *Sci. Total Environ.* **2016**, *545–546*, 48–56. [[CrossRef](#)]
41. Du, L.; Zhao, Y.; Wang, C.; Zhang, H.; Chen, Q.; Zhang, X.; Zhang, L.; Wu, J.; Wu, Z.; Zhou, Q. Removal performance of antibiotics and antibiotic resistance genes in swine wastewater by integrated vertical-flow constructed wetlands with zeolite substrate. *Sci. Total Environ.* **2020**, *721*, 137765. [[CrossRef](#)]
42. Chen, J.; Xie, S. Overview of sulfonamide biodegradation and the relevant pathways and microorganisms. *Sci. Total Environ.* **2018**, *640–641*, 1465–1477. [[CrossRef](#)]
43. Kovalakova, P.; Cizmas, L.; McDonald, T.J.; Marsalek, B.; Feng, M.; Sharma, V.K. Occurrence and toxicity of antibiotics in the aquatic environment: A review. *Chemosphere* **2020**, *251*, 126351. [[CrossRef](#)] [[PubMed](#)]
44. Nsenga Kumwimba, M.; Meng, F. Roles of ammonia-oxidizing bacteria in improving metabolism and cometabolism of trace organic chemicals in biological wastewater treatment processes: A review. *Sci. Total Environ.* **2019**, *659*, 419–441. [[CrossRef](#)] [[PubMed](#)]
45. Popa, C.; Favier, L.; Dinica, R.; Semrany, S.; Djelal, H.; Amrane, A.; Bahrim, G. Potential of newly isolated wild Streptomyces strains as agents for the biodegradation of a recalcitrant pharmaceutical, carbamazepine. *Environ. Technol.* **2014**, *35*, 3082–3091. [[CrossRef](#)] [[PubMed](#)]
46. Zhang, J.-J.; Chen, Y.-F.; Fang, T.; Zhou, N.-Y. Co-metabolic degradation of tribenuron methyl, a sulfonylurea herbicide, by *Pseudomonas* sp. strain NyZ42. *Int. Biodeterior. Biodegrad.* **2013**, *76*, 36–40. [[CrossRef](#)]
47. Domaradzka, D.; Guzik, U.; Hupert-Kocurek, K.; Wojcieszynska, D. Cometabolic Degradation of Naproxen by *Planococcus* sp. Strain S5. *Water Air Soil Pollut.* **2015**, *226*, 297. [[CrossRef](#)]
48. Xie, S.; Liu, J.; Li, L.; Qiao, C. Biodegradation of malathion by *Acinetobacter johnsonii* MA19 and optimization of cometabolism substrates. *J. Environ. Sci.* **2009**, *21*, 76–82. [[CrossRef](#)]
49. Pant, D.; Van Bogaert, G.; Diels, L.; Vanbroekhoven, K. A review of the substrates used in microbial fuel cells (MFCs) for sustainable energy production. *Bioresour. Technol.* **2010**, *101*, 1533–1543. [[CrossRef](#)]
50. Wang, H.; Heil, D.; Ren, Z.J.; Xu, P. Removal and fate of trace organic compounds in microbial fuel cells. *Chemosphere* **2015**, *125*, 94–101. [[CrossRef](#)]
51. Fadzli, F.S.; Bhawani, S.A.; Adam Mohammad, R.E.; Maneiro, M. Microbial Fuel Cell: Recent Developments in Organic Substrate Use and Bacterial Electrode Interaction. *J. Chem.* **2021**, *2021*, 4570388. [[CrossRef](#)]

52. Wang, J.; Song, X.; Wang, Y.; Bai, J.; Li, M.; Dong, G.; Lin, F.; Lv, Y.; Yan, D. Bioenergy generation and rhizodegradation as affected by microbial community distribution in a coupled constructed wetland-microbial fuel cell system associated with three macrophytes. *Sci. Total Environ.* **2017**, *607–608*, 53–62. [[CrossRef](#)]
53. Fang, Z.; Song, H.-l.; Cang, N.; Li, X.-n. Electricity production from Azo dye wastewater using a microbial fuel cell coupled constructed wetland operating under different operating conditions. *Biosens. Bioelectron.* **2015**, *68*, 135–141. [[CrossRef](#)] [[PubMed](#)]
54. Hijosa-Valsero, M.; Reyes-Contreras, C.; Domínguez, C.; Bécares, E.; Bayona, J.M. Behaviour of pharmaceuticals and personal care products in constructed wetland compartments: Influent, effluent, pore water, substrate and plant roots. *Chemosphere* **2016**, *145*, 508–517. [[CrossRef](#)] [[PubMed](#)]
55. Li, H.; Xu, H.; Song, H.-L.; Lu, Y.; Yang, X.-L. Antibiotic resistance genes, bacterial communities, and functions in constructed wetland-microbial fuel cells: Responses to the co-stresses of antibiotics and zinc. *Environ. Pollut.* **2020**, *265*, 115084. [[CrossRef](#)] [[PubMed](#)]
56. APHA. *Standard Methods for the Examination of Water and Wastewater*, 23rd ed.; American Public Health Association: Washington, DC, USA; American Water Works Association: Washington, DC, USA, 2018.
57. Fang, Z.; Song, H.L.; Yu, R.; Li, X.N. A microbial fuel cell-coupled constructed wetland promotes degradation of azo dye decolorization products. *Ecol. Eng.* **2016**, *94*, 455–463. [[CrossRef](#)]
58. Bokulich, N.A.; Subramanian, S.; Faith, J.J.; Gevers, D.; Gordon, J.I.; Knight, R.; Mills, D.A.; Caporaso, J.G. Quality-filtering vastly improves diversity estimates from Illumina amplicon sequencing. *Nat. Methods* **2013**, *10*, 57–59. [[CrossRef](#)]
59. Fang, Z.; Song, H.-L.; Cang, N.; Li, X.-N. Performance of microbial fuel cell coupled constructed wetland system for decolorization of azo dye and bioelectricity generation. *Bioresour. Technol.* **2013**, *144*, 165–171. [[CrossRef](#)]
60. Yi, X.; Tran, N.H.; Yin, T.; He, Y.; Gin, K.Y.-H. Removal of selected PPCPs, EDCs, and antibiotic resistance genes in landfill leachate by a full-scale constructed wetlands system. *Water Res.* **2017**, *121*, 46–60. [[CrossRef](#)]
61. Stülten, D.; Zühlke, S.; Lamshöft, M.; Spitteller, M. Occurrence of diclofenac and selected metabolites in sewage effluents. *Sci. Total Environ.* **2008**, *405*, 310–316. [[CrossRef](#)]
62. Yang, Y.; Wang, Z.; He, T.; Dai, Y.; Xie, S. Sediment bacterial communities associated with anaerobic biodegradation of bisphenol A. *Microb. Ecol.* **2015**, *70*, 97–104. [[CrossRef](#)]
63. Zhang, L.; Liu, Y.; Lv, S.; Wang, R.; Wang, Y.; Lin, K.; Hu, X.; Liu, Y.; Dong, Z.; Liu, L. An overview on constructed wetland-microbial fuel cell: Greenhouse gases emissions and extracellular electron transfer. *J. Environ. Chem. Eng.* **2023**, *11*, 109551. [[CrossRef](#)]
64. Logan, B.E.; Regan, J.M. Microbial Fuel Cells—Challenges and Applications. *Environ. Sci. Technol.* **2006**, *40*, 5172–5180. [[CrossRef](#)] [[PubMed](#)]
65. Xia, Z.; Xiao-chun, W.; Zhong-lin, C.; Hao, X.; Qing-fang, Z. Microbial community structure and pharmaceuticals and personal care products removal in a membrane bioreactor seeded with aerobic granular sludge. *Appl. Microbiol. Biotechnol.* **2015**, *99*, 425–433. [[CrossRef](#)] [[PubMed](#)]
66. Xu, F.; Cao, F.Q.; Kong, Q.; Zhou, L.L.; Yuan, Q.; Zhu, Y.J.; Wang, Q.; Du, Y.D.; Wang, Z.D. Electricity production and evolution of microbial community in the constructed wetland-microbial fuel cell. *Chem. Eng. J.* **2018**, *339*, 479–486. [[CrossRef](#)]
67. Zhu, C.-Y.; Wang, J.-F.; Li, Q.-S.; Wang, L.-L.; Tang, G.-H.; Cui, B.-S.; Bai, J. Integration of CW-MFC and anaerobic granular sludge to explore the intensified ammonification-nitrification-denitrification processes for nitrogen removal. *Chemosphere* **2021**, *278*, 130428. [[CrossRef](#)] [[PubMed](#)]
68. Yang, Q.; Wu, Z.X.; Liu, L.F.; Zhang, F.X.; Liang, S.N. Treatment of Oil Wastewater and Electricity Generation by Integrating Constructed Wetland with Microbial Fuel Cell. *Materials* **2016**, *9*, 885. [[CrossRef](#)]
69. Silambarasan, S.; Abraham, J. Biodegradation of carbendazim by a potent novel *Chryseobacterium* sp. JAS14 and plant growth promoting *Aeromonas caviae* JAS15 with subsequent toxicity analysis. *3 Biotech* **2020**, *10*, 326. [[CrossRef](#)]
70. Zhang, W.; Li, J.; Zhang, Y.; Wu, X.; Zhou, Z.; Huang, Y.; Zhao, Y.; Mishra, S.; Bhatt, P.; Chen, S. Characterization of a novel glyphosate-degrading bacterial species, *Chryseobacterium* sp. Y16C, and evaluation of its effects on microbial communities in glyphosate-contaminated soil. *J. Hazard. Mater.* **2022**, *432*, 128689. [[CrossRef](#)]
71. Figueroa, D.; Capo, E.; Lindh, M.V.; Rowe, O.F.; Paczkowska, J.; Pinhassi, J.; Andersson, A. Terrestrial dissolved organic matter inflow drives temporal dynamics of the bacterial community of a subarctic estuary (northern Baltic Sea). *Env. Microbiol* **2021**, *23*, 4200–4213. [[CrossRef](#)]
72. Xu, B.; Gao, P.; Liu, Z.; Xue, G.; Liu, Y.; Wu, F. Influence of Cosubstrates on Iopromide Degradation by *Pseudomonas* sp. I-24. *Water Air Soil Pollut.* **2014**, *225*, 1849. [[CrossRef](#)]
73. Lawson, K. Emerging pharmacological strategies for the treatment of fibromyalgia. *World J. Pharmacol.* **2017**, *6*, 1–10. [[CrossRef](#)]
74. Liu, C.; Liu, T.; Zheng, X.; Meng, J.; Chen, H.; Yuan, Z.; Hu, S.; Guo, J. Rapid formation of granules coupling n-DAMO and anammox microorganisms to remove nitrogen. *Water Res.* **2021**, *194*, 116963. [[CrossRef](#)] [[PubMed](#)]
75. Corbella, C.; Guivernau, M.; Vinas, M.; Puigagut, J. Operational, design and microbial aspects related to power production with microbial fuel cells implemented in constructed wetlands. *Water Res.* **2015**, *84*, 232–242. [[CrossRef](#)] [[PubMed](#)]
76. Huang, X.; Zheng, J.; Liu, C.; Liu, L.; Liu, Y.; Fan, H.; Zhang, T. Performance and bacterial community dynamics of vertical flow constructed wetlands during the treatment of antibiotics-enriched swine wastewater. *Chem. Eng. J.* **2017**, *316*, 727–735. [[CrossRef](#)]

77. Zhao, X.; Chen, Z.; Wang, X.; Li, J.; Shen, J.; Xu, H. Remediation of pharmaceuticals and personal care products using an aerobic granular sludge sequencing bioreactor and microbial community profiling using Solexa sequencing technology analysis. *Bioresour. Technol.* **2015**, *179*, 104–112. [[CrossRef](#)]
78. Vymazal, J. Constructed wetlands for wastewater treatment. *Ecol. Eng.* **2005**, *25*, 475–477. [[CrossRef](#)]
79. Oon, Y.L.; Ong, S.A.; Ho, L.N.; Wong, Y.S.; Dahalan, F.A.; Oon, Y.S.; Teoh, T.P.; Lehl, H.K.; Thung, W.E. Constructed wetland-microbial fuel cell for azo dyes degradation and energy recovery: Influence of molecular structure, kinetics, mechanisms and degradation pathways. *Sci. Total Environ.* **2020**, *720*, 15. [[CrossRef](#)]
80. Song, H.L.; Zhang, S.; Guo, J.H.; Yang, Y.L.; Zhang, L.M.; Li, H.; Yang, X.L.; Liu, X. Vertical up-flow constructed wetlands exhibited efficient antibiotic removal but induced antibiotic resistance genes in effluent. *Chemosphere* **2018**, *203*, 434–441. [[CrossRef](#)]
81. Ebrahimi, A.; Sivakumar, M.; McLauchlan, C.; Ansari, A.; Vishwanathan, A.S. A critical review of the symbiotic relationship between constructed wetland and microbial fuel cell for enhancing pollutant removal and energy generation. *J. Environ. Chem. Eng.* **2021**, *9*, 105011. [[CrossRef](#)]
82. Sonawane, J.M.; Yadav, A.; Ghosh, P.C.; Adeloju, S.B. Recent advances in the development and utilization of modern anode materials for high performance microbial fuel cells. *Biosens. Bioelectron.* **2017**, *90*, 558–576. [[CrossRef](#)]
83. Sizerici, B.; Yildiz, I. Simultaneous removal of organics and metals in fixed bed using gravel and iron oxide coated gravel. *Results Eng.* **2020**, *5*, 100093. [[CrossRef](#)]
84. Oon, Y.-L.; Ong, S.-A.; Ho, L.-N.; Wong, Y.-S.; Dahalan, F.A.; Oon, Y.-S.; Lehl, H.K.; Thung, W.-E. Synergistic effect of up-flow constructed wetland and microbial fuel cell for simultaneous wastewater treatment and energy recovery. *Bioresour. Technol.* **2016**, *203*, 190–197. [[CrossRef](#)] [[PubMed](#)]
85. Zhao, C.C.; Shang, D.W.; Zou, Y.L.; Du, Y.D.; Wang, Q.; Xu, F.; Ren, L.; Kong, Q. Changes in electricity production and microbial community evolution constructed wetland -microbial fuel cell exposed to wastewater containing Pb(II). *Sci. Total Environ.* **2020**, *732*, 11. [[CrossRef](#)] [[PubMed](#)]
86. González, T.; Puigagut, J.; Vidal, G. Organic matter removal and nitrogen transformation by a constructed wetland-microbial fuel cell system with simultaneous bioelectricity generation. *Sci. Total Environ.* **2021**, *753*, 142075. [[CrossRef](#)]
87. Wu, D.; Yang, L.Y.; Gan, L.; Chen, Q.K.; Li, L.; Chen, X.; Wang, X.; Guo, L.Y.; Miao, A.J. Potential of novel wastewater treatment system featuring microbial fuel cell to generate electricity and remove pollutants. *Ecol. Eng.* **2015**, *84*, 624–631. [[CrossRef](#)]
88. Saz, Ç.; Türe, C.; Türker, O.C.; Yakar, A. Effect of vegetation type on treatment performance and bioelectric production of constructed wetland modules combined with microbial fuel cell (CW-MFC) treating synthetic wastewater. *Environ. Sci. Pollut. Res.* **2018**, *25*, 8777–8792. [[CrossRef](#)]
89. Araneda, I.; Tapia, N.F.; Allende, K.L.; Vargas, I.T. Constructed Wetland-Microbial Fuel Cells for Sustainable Greywater Treatment. *Water* **2018**, *10*, 940. [[CrossRef](#)]
90. Liu, Q.; Zhou, B.X.; Zhang, S.C.; Xu, D.; Pan, R.; Xia, S.B. Embedding Microbial Fuel Cells into the Vertical Flow Constructed Wetland Enhanced Denitrogenation and Water Purification. *Pol. J. Environ. Stud.* **2019**, *28*, 1799–1804. [[CrossRef](#)]
91. Zhang, S.; Song, H.-L.; Yang, X.-L.; Li, H.; Wang, Y.-W. A system composed of a biofilm electrode reactor and a microbial fuel cell-constructed wetland exhibited efficient sulfamethoxazole removal but induced sul genes. *Bioresour. Technol.* **2018**, *256*, 224–231. [[CrossRef](#)]
92. Pepè Sciarria, T.; Arioli, S.; Gargari, G.; Mora, D.; Adani, F. Monitoring microbial communities' dynamics during the start-up of microbial fuel cells by high-throughput screening techniques. *Biotechnol. Rep.* **2019**, *21*, e00310. [[CrossRef](#)]
93. Zhang, L.; Zhu, X.; Li, J.; Liao, Q.; Ye, D. Biofilm formation and electricity generation of a microbial fuel cell started up under different external resistances. *J. Power Sources* **2011**, *196*, 6029–6035. [[CrossRef](#)]
94. Chae, K.-J.; Choi, M.-J.; Lee, J.-W.; Kim, K.-Y.; Kim, I.S. Effect of different substrates on the performance, bacterial diversity, and bacterial viability in microbial fuel cells. *Bioresour. Technol.* **2009**, *100*, 3518–3525. [[CrossRef](#)] [[PubMed](#)]
95. Dong, X.; Li, D.; Li, Y.; Sakiyama, H.; Muddassir, M.; Pan, Y.; Srivastava, D.; Kumar, A. A 3,8-connected Cd(ii)-based metal-organic framework as an appropriate luminescent sensor for the antibiotic sulfasalazine. *CrystEngComm* **2022**, *24*, 7157–7165. [[CrossRef](#)]
96. Bin, H.-S.; Hu, H.; Wang, J.; Lu, L.; Muddassir, M.; Srivastava, D.; Chauhan, R.; Wu, Y.; Wang, X.; Kumar, A. New 5,5-(1,4-Phenylenebis(methyleneoxy)diisophthalic Acid Appended Zn(II) and Cd(II) MOFs as Potent Photocatalysts for Nitrophenols. *Molecules* **2023**, *28*, 7180. [[CrossRef](#)] [[PubMed](#)]

Disclaimer/Publisher's Note: The statements, opinions and data contained in all publications are solely those of the individual author(s) and contributor(s) and not of MDPI and/or the editor(s). MDPI and/or the editor(s) disclaim responsibility for any injury to people or property resulting from any ideas, methods, instructions or products referred to in the content.